Biomimetic Periodontal Ligament Transplantation Activated by Gold Nanoparticles Protects Alveolar Bone

Chen Zong[1], Wannes Van Holm[2], Annelies Bronckaers[3], Zuodong Zhao[1], Stevan Čokić[4], Merve Kübra Akta[5], Ana Belén Castro[2], Bart Van Meerbeek[4], Annabel Braem[5], Guy Willems[1], Maria Cadenas de Llano-Pérula[1]*

[1]KU Leuven (University of Leuven), Department of Oral Health Sciences, Orthodontics and UZ Leuven (University Hospitals Leuven), Dentistry, Leuven, Belgium.

[2]KU Leuven, Department of Oral Health Sciences, Periodontology & Oral Microbiology and UZ Leuven, Dentistry, Leuven, Belgium.

[3]University of Hasselt, Faculty of Life Sciences, Biomedical Research Institute, Diepenbeek, Belgium.

[4]Department of Oral Health Sciences-BIOMAT, University of Leuven (KU Leuven) and UZ Leuven, Dentistry, Leuven, Belgium.

[5]KU Leuven, Department of Materials Engineering (MTM), Biomaterials and Tissue Engineering Research Group, Leuven, Belgium

*Corresponding author

Chen Zong

KU Leuven (University of Leuven), Department of Oral Health Sciences, Orthodontics and UZ Leuven (University Hospitals Leuven), Dentistry, Kapucijnenvoer 7, blok A bus 7001, 3000 Leuven, Belgium

E-mail: chen.zong@kuleuven.be

Abstract

Stem cell therapy might be a promising method to stimulate alveolar bone regeneration, which is currently a major clinical challenge. However, its therapeutic features largely depend on pretreatment and transplantation preparation. Herein, a novel biomimetic periodontal ligament transplantation composed of human periodontal ligament stem cells (hPDLSCs) pretreated with gold nanocomplexes (AuNCs) and embedded in a type-I collagen hydrogel scaffold is developed to protect alveolar bone from resorption. AuNCs were readily absorbed by primary hPDLSCs, with limited cytotoxicity, and promoted osteogenic differentiation of hPDLSCs effectively *in vitro*. In addition, the AuNCs-induced hPDLSCs were encapsulated with type-I collagen hydrogel scaffold to mimic their native physiological niche, and then transplanted into a rat model of alveolar bone resorption. Both micro-computed tomography (micro-CT) and immunohistochemical assays demonstrated that alveolar bone loss was significantly prevented. Furthermore, the underlying therapeutic mechanism was elucidated, in which transplantation-activated osteogenesis was associated with autophagy, which enabled bone remodeling and regeneration. This study provides critical insight into the role of PDLSCs in bone homeostasis and proposes an innovative AuNCs-based strategy for stem cell therapy in bone regeneration.

Keywords

Gold nanoparticles, stem cell transplantation, autophagy, periodontal ligament, bone regeneration, tooth movement, alveolar bone.

1. Introduction

Alveolar bone loss has long been a significant issue in dentistry due to its irreversible nature leading to gingival recession, exposed dental roots and eventual tooth loss. Generalized tooth loss can lead to the bite collapsing, which strongly affects the vertical height of the lower third of the face. These can directly affect a patient's quality of life by impairing their ability to properly masticate, speak and even socialize[1]. Therefore, developing an effective approach to protect alveolar bone is of great interest to both clinicians and patients. Autologous and allogenic alveolar bone grafts are the most common and traditional treatments for overcoming bone defects and atrophy. Although they are currently regarded as the therapeutic gold standard, these methods present complications such as donor site morbidity, graft failure, immunological rejection, limited source of graft tissue and lengthy hospitalization periods[2]. To avoid these complications, novel tissue engineering techniques and stem cell-based regenerative therapies for bone regeneration are being investigated more frequently. Mesenchymal stem cells (MSCs) are crucial regulators of tissue homeostasis and support tissue integrity[3]. The transplantation of mesenchymal stem cells (MSCs) combined with engineering scaffolds demonstrated great potential for the regeneration of multiple tissues, such as bone, cartilage, skin, liver and nerves[4]. Nevertheless, despite the remarkable results achieved already, the translation of therapeutic outcomes from the laboratory bench to the patient's bedside remains an arduous challenge[5].

Firstly, the lack of clinical application of MSCs could be attributed to their poor quality and the inconsistency of their therapeutic features, such as self-renewal, differentiation immunocompatibility, genomic stability, heterogeneity and migratory capacity[6, 7]. Numerous attempts have been made to overcome these limitations, including the use of cell-free conditional culture medium[8] or extracellular vesicles such as exosomes[9]. However, due to factors such as low production, lack of standards for quality control and risk of contamination, the application of these methods remains limited[10]. To enhance the therapeutic properties and reduce the variability of MSCs (and their derived products), it is necessary to consider the conditions of potential donors and their native physiological niches[11]. Therefore, a correct selection of MSCs based on their functional potential is essential for optimizing therapeutic properties in artificial niches[12]. Bone marrow stem cells (BMSCs) and periodontal ligament stem cells (PDLSCs) are very suitable for alveolar bone regeneration, as they originally reside in the periodontium. However, BMSCs are sourced from bone marrow, which can restrict their

availability. In contrast, due to their origin being from the periodontium, PDLSCs are readily available throughout the entire human lifespan[13, 14], and have demonstrated regenerative capacities in multiple tissues[15-17], making them an ideal source of MSCs for the treatment or prevention of alveolar bone loss.

Secondly, prolonged *in vitro* culture and passage of MSCs may lead to decreased expression levels of specific surface antigens, abnormal morphology, self-renewal capacity, proliferation rate and accelerated senescence[18]. The loss of stemness often hinders the therapeutic properties of MSCs, resulting in the failure of MSC transplantation[19]. Customized pretreatment of the MSCs with chemical agents[20], hypoxia[21] or gene modifications[22] may reactivate the MSCs and enhance their tissue regeneration capacity. The rationale for the selected pretreatment depends on the specific type of MSCs and the targeted tissue. Gold nanoparticles (AuNPs) may be a promising pretreatment for PDLSCs, as they have been used for cellular tracking of PDLSCs with minimal cytotoxicity[23] and are able to induce autophagy[24, 25]. Autophagy is essential for the maintenance of cellular homeostasis and differentiation under hostile conditions[26], which can determine the fate of MSCs[27] and subsequently promote bone regeneration in turn[28].

Third, the engineering scaffold has a pivotal role to ensure the survival of MSCs in the complex physiological microenvironment where it is transplanted. The scaffold should provide optimal conditions to sustain MSC growth and differentiation, extracellular matrix deposition, and the formation of new bone [29]. However, synthetic scaffolds can also have adverse effects *in vivo* by reducing cell viability[30] and inducing inflammation compared to natural materials[31]. Although scaffold-free approaches such as cell sheet technology, which can promote cellular self-assembly, may be a viable alternative, they are limited by poor mechanical properties, spontaneous contraction and shrinkage of cell sheets[32]. Consequently, selecting the appropriate engineering scaffold for protecting or regenerating the alveolar bone remains a staggering challenge.

The current study aims to develop a novel, yet straightforward approach to protecting alveolar bone using biomimetic periodontal ligament transplantation activated by AuNCs. To test this strategy *in vivo*, a validated orthodontic animal model was used[33], as orthodontic tooth movement is essentially a process of aseptic inflammation that leads to alveolar bone resorption. This method to investigate bone regeneration has several advantages over other models of

alveolar bone loss induced by infection, trauma, tooth loss or surgically-inflicted defects. This innovative approach might create a new field for the autotransplantation of hPDLSCs, which could benefit millions of patients.

2. Results

2.1 Isolation and characterization of hPDLSCs

Periodontal ligament cells were isolated from the extracted teeth of six healthy young patients by the outgrowth method. The hPDLSCs were screened for the expression of specific surface antigens by flow cytometry analysis (positive: CD29, CD44, CD73, CD90 and CD105, negative: CD31, CD34, CD45). Their MSC properties matched the criteria of the International Society for Cellular Therapy[34]: colony-forming unit, cell-doubling time, cell viability and osteogenic differentiation assay (**Figure 1**). All experiments in this study were conducted with hPDLSCs between passages 2 and 6.

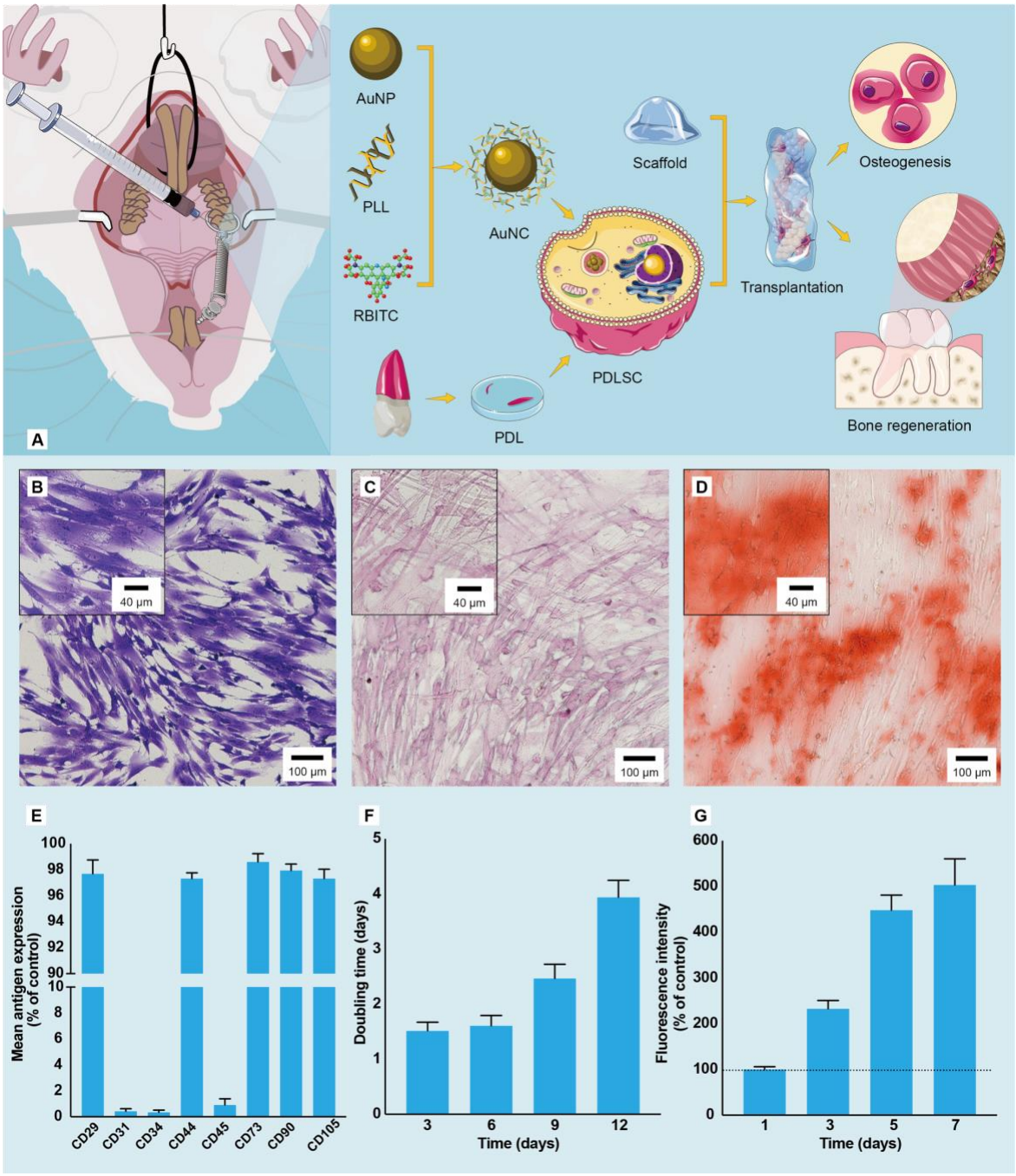

Figure 1. Characterization of hPDLSCs.

A) Graphical visualization of the performed experiments. B) *In vitro* cell proliferation is shown with a light microscope. C, D) The osteogenic differentiation capacity of the cells is confirmed with alkaline phosphatase staining and detection of alizarin red-positive calcium nodules. E) Mean expression level of the specific surface antigen of hPDLSCs ± standard deviation (SD) (n = 6). CD: cluster of differentiation. F) Mean proliferation rate of hPDLSCs ± SD (n = 3). G) Mean viability of hPDLSCs over time ± SD (n = 30).

2.2. Synthesis of AuNCs for cellular uptake by hPDLSCs

AuNCs (AuNP–Poly-L-lysine hydrobromide–rhodamine B isothiocyanate) were freshly prepared as previously described[23]. Afterward, their spherical morphology, particle diameter, size distribution, zeta potential and surface features were characterized by high-resolution transmission electron microscopy (TEM), scanning electron microscopy (SEM), dynamic light scattering (DLS) and electrophoretic light scattering (ELS), respectively.

The results of particle diameter, size distribution and zeta potential or AuNCs (mean ± SD) are shown in **Figure 2 (G-I)**. First, the particle diameter measured using TEM conformed to a Gaussian distribution, averaging 39.8 nm (n = 200). Second, 40nm AuNPs tended to aggregate after preparation for 24 h, which was reflected by the intensity-based result of DLS analysis and TEM. In contrast, the intensity-weighted distribution measured using DLS is susceptible to small numbers of aggregates, as scattering intensity from a spherical particle is equivalent to the size of the 6^{th} power. Third, the naked AuNPs have a negative surface charge, which might restrict their cellular uptake, as the cell membrane is also negatively charged. Therefore, AuNPs were coated with Poly-L-lysine hydrobromide (PLL), a cationic transfection agent which granted AuNCs a positive surface charge to enhance endocytosis efficiency.

Subsequently, hPDLSCs were treated with culture medium (CM) containing 0.1 mg/mL AuNCs for 12 h. The cellular uptake of AuNCs was verified by TEM, SEM and fluorescence microscopy, as shown in **Figure 2 (A-F)**. The TEM showed that the particles were ingested through endocytosis, as the AuNCs appeared in the intracellular vesicles. The SEM, brightfield and fluorescence microscopy confirmed the existence of AuNCs and uptake in the cytoplasm of hPDLSCs. Thus, CM containing 0.1 mg/mL AuNCs enabled an efficient uptake by the hPDLSCs.

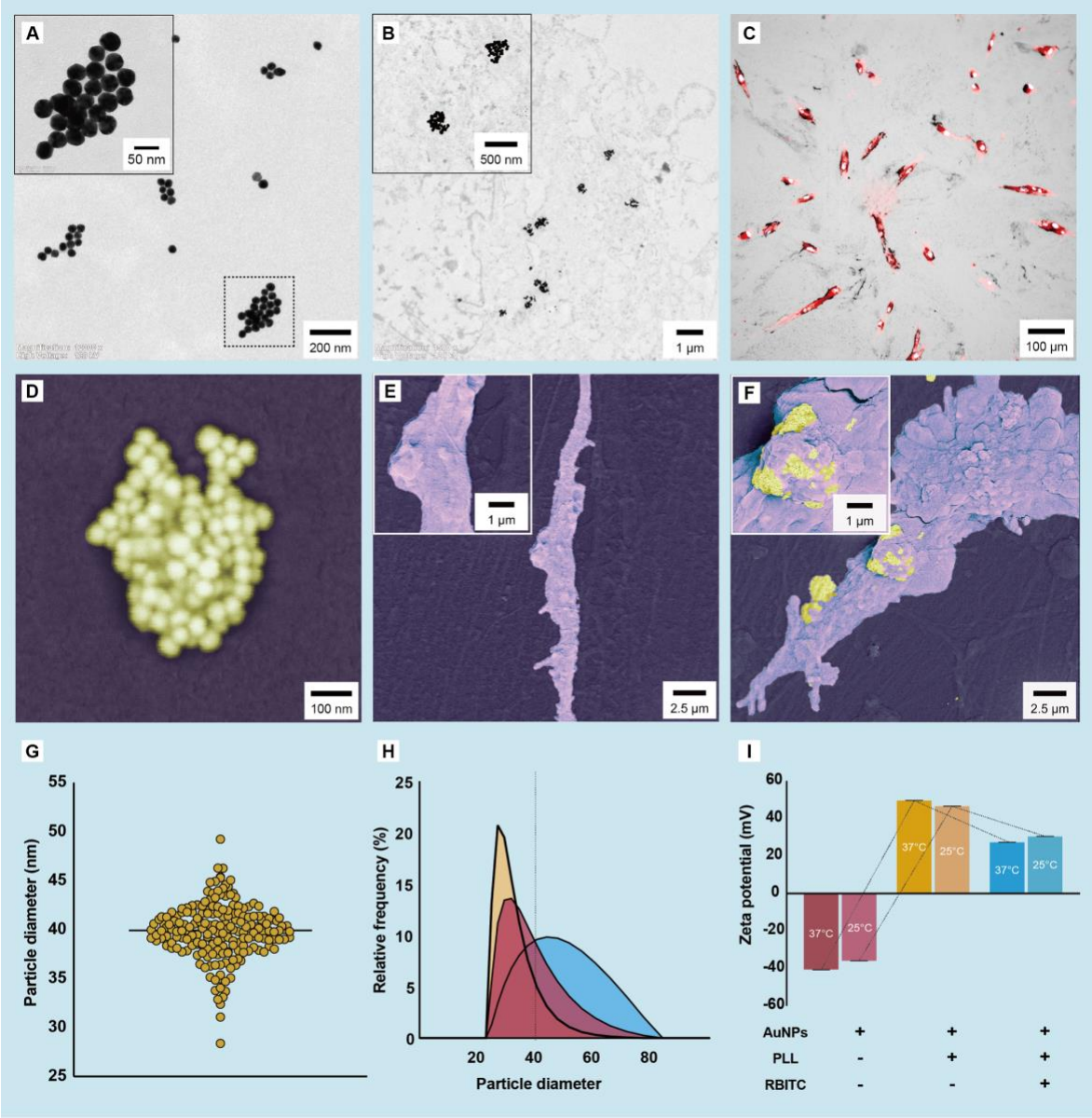

Figure 2. Characterization and cellular uptake of AuNCs.

A) The spherical morphology and particle diameter of AuNCs evaluated with TEM. B) The cellular uptake of AuNCs by endocytosis observed with TEM. C) The fluorescence of hPDLSCs rendered by AuNCs, as shown by fluorescence microscopy. D, E, F) The surface feature of non-uptake AuNCs and hPDLSCs without or with AuNCs visualized with SEM. G) Mean particle diameter of AuNCs ± SD (n = 200). H) Size distribution of AuNCs (n = 100) determined by particle volume (red), number (yellow) and intensity (blue). I) Mean zeta potential of naked AuNPs (red), AuNP-PLL (yellow) and AuNP-PLL-RBITC (blue) ± SD (n = 100) at 37°C or 25°C, respectively.

2.3. Gold nanocomplexes (AuNCs) promote hPDLSCs osteogenic differentiation

To evaluate whether AuNCs can alter the osteogenic differentiation capacity, the hPDLSCs were cultured in 24-well plates and divided into four different groups: cells cultured in CM without AuNCs, CM with 0.1 mg/mL AuNCs, osteogenic medium (OM) without AuNCs, and OM with 0.1 mg/mL AuNCs. A series of experiments were performed to assess and compare the osteogenic differentiation capacity of those hPDLSCs in mentioned conditions.

The ALP and ARS staining showed that 0.1 mg/mL AuNCs increased the osteogenic functionality of hPDLSCs, independent from the presence of OM ($p < 0.05$). This result was further confirmed by IF staining, which showed that AuNCs enhanced the ALP expression of hPDLSCs ($p < 0.05$). Additionally, reverse transcription-quantitative polymerase chain reaction (RT-qPCR) showed that AuNCs significantly upregulated the gene expression of two representative osteogenic markers, COL1 and OSTERIX ($p < 0.05$). In summary, AuNCs promoted the osteogenic differentiation of hPDLSCs at multiple levels (**Figure 3**).

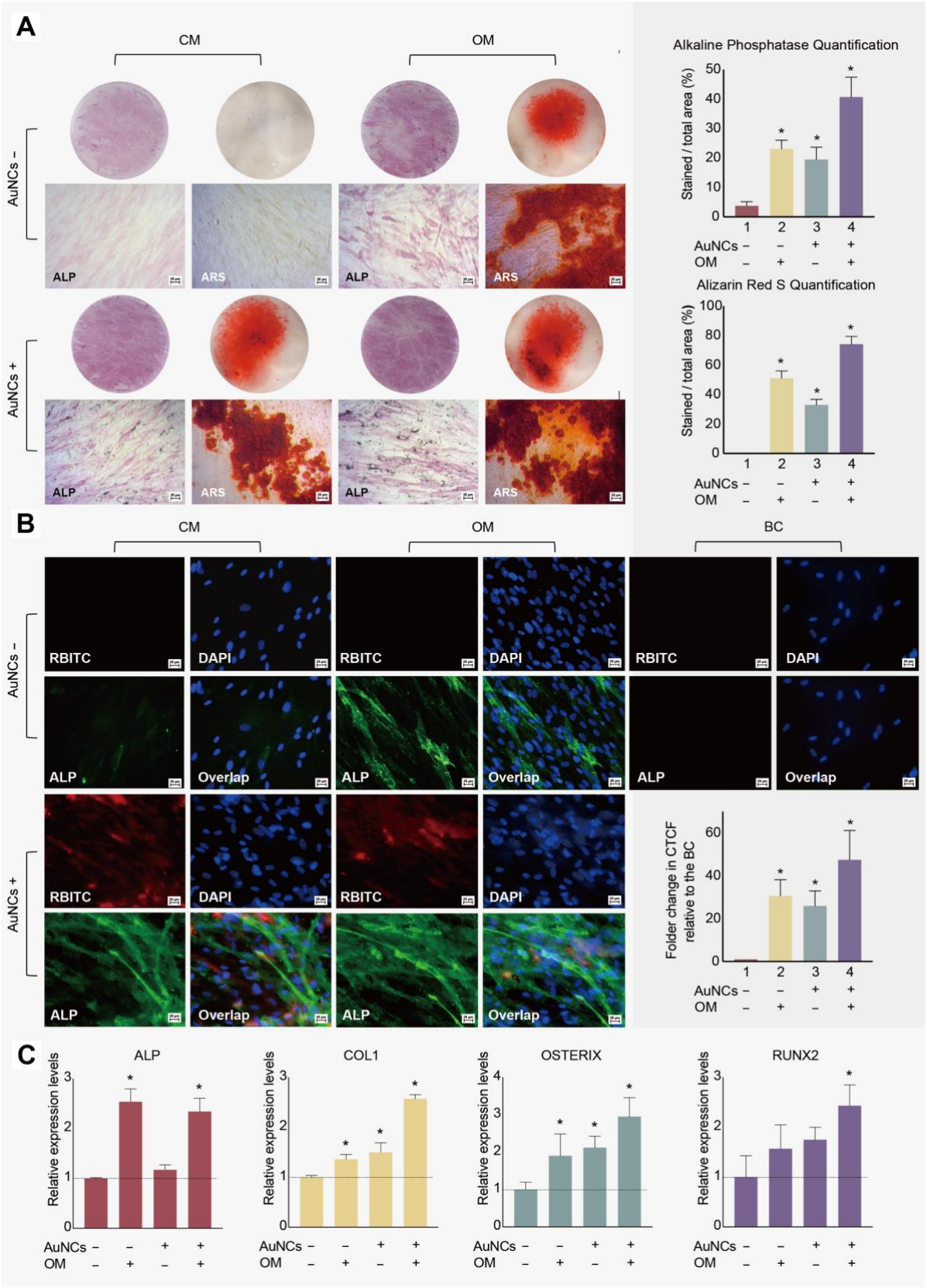

Figure 3. Influence of AuNCs on the osteogenic differentiation capacity of hPDLSC.

A) The ALP activity and mineralized nodule formation assessed by ALP and ARS staining show that AuNCs can increase osteogenic functionality at the protein expression level. The

histograms show the quantification of ALP and ARS by ImageJ analysis (n = 6). B) The colocalization of RBITC, DAPI, and ALP also shows that AuNCs can enhance the ALP expression. BC (blank control) refers to the cells cultured without AuNCs and with only secondary AF488-labeled antibody. Scale bar = 20 μm. The histogram shows the folder changes in ALP fluorescence intensity of the cells treated with different conditions relative to the BC by ImageJ analysis (n = 6). CTCF: corrected total cell fluorescence. C) The RT-qPCR shows that AuNCs can promote the gene expression of osteogenic markers. The histograms show the relative expression levels of the cells treated with different conditions relative to those cultured in CM without AuNCs. All the above data were analyzed with one-way ANOVA and expressed as the mean (n = 6) with SD error bars. *$p < 0.05$ versus hPDLSC cultured in CM without AuNCs.

2.4. AuNCs-induced osteogenic differentiation is associated with autophagy

To investigate the involvement of autophagy in AuNC-induced osteogenic differentiation, ALP and ARS staining were repeated. The hPDLSCs with or without AuNCs were also exposed to the autophagy inhibitor chloroquine (0.5 μM) and autophagy enhancer rapamycin (4 μM). High-resolution TEM was used to detect the autophagosomes. A cell cytotoxicity assay by Alamarblue HS cell viability reagent was used to evaluate the AuNC-induced change in cell viability. Subsequently, the gene expression of autophagy markers LC3 and P62 and osteogenic markers ALP, COL1, OSTERIX and RUNX2 were analyzed by RT-qPCR.

The ALP and ARS staining showed that rapamycin and chloroquine could promote and inhibit osteogenic differentiation, respectively. When applied in combination with AuNCs, they further strengthened or impaired the AuNCs-induced osteogenesis, respectively (**Figure 4A, B, C**). Meanwhile, the TEM verified the existence of the double-membrane autophagosomes accumulated in hPDLSCs treated with AuNCs and located their intracellular positions (**Figure 4D**). By comparing the cells treated with rapamycin (positive control) and those treated with chloroquine (negative control), the cells incubated with AuNCs demonstrated that AuNCs induced autophagy. Besides, no AuNCs were found in the nuclei.

Furthermore, although the AuNCs could induce cell autophagy, the cell cytotoxicity assay indicated that 0.1 mg/mL AuNCs had no statistically significant impact on hPDLSCs viability after 7 days (**Figure 4E**).

The RT-qPCR results showed that AuNCs acted similarly to rapamycin, which activated autophagy. This was observed as the upregulation of the gene expression of LC3 and the downregulation of P62 (1.42±0.18 fold and 0.68±0.10 fold, respectively). This process was

concomitant with the upregulation of the gene expression of the osteogenic markers COL1, OSTERIX and RUNX2 (**Figure 4F, G**). In contrast, chloroquine treatment reversed the activation of autophagy by AuNCs-upregulated gene expression of the osteogenic markers ($p < 0.05$).

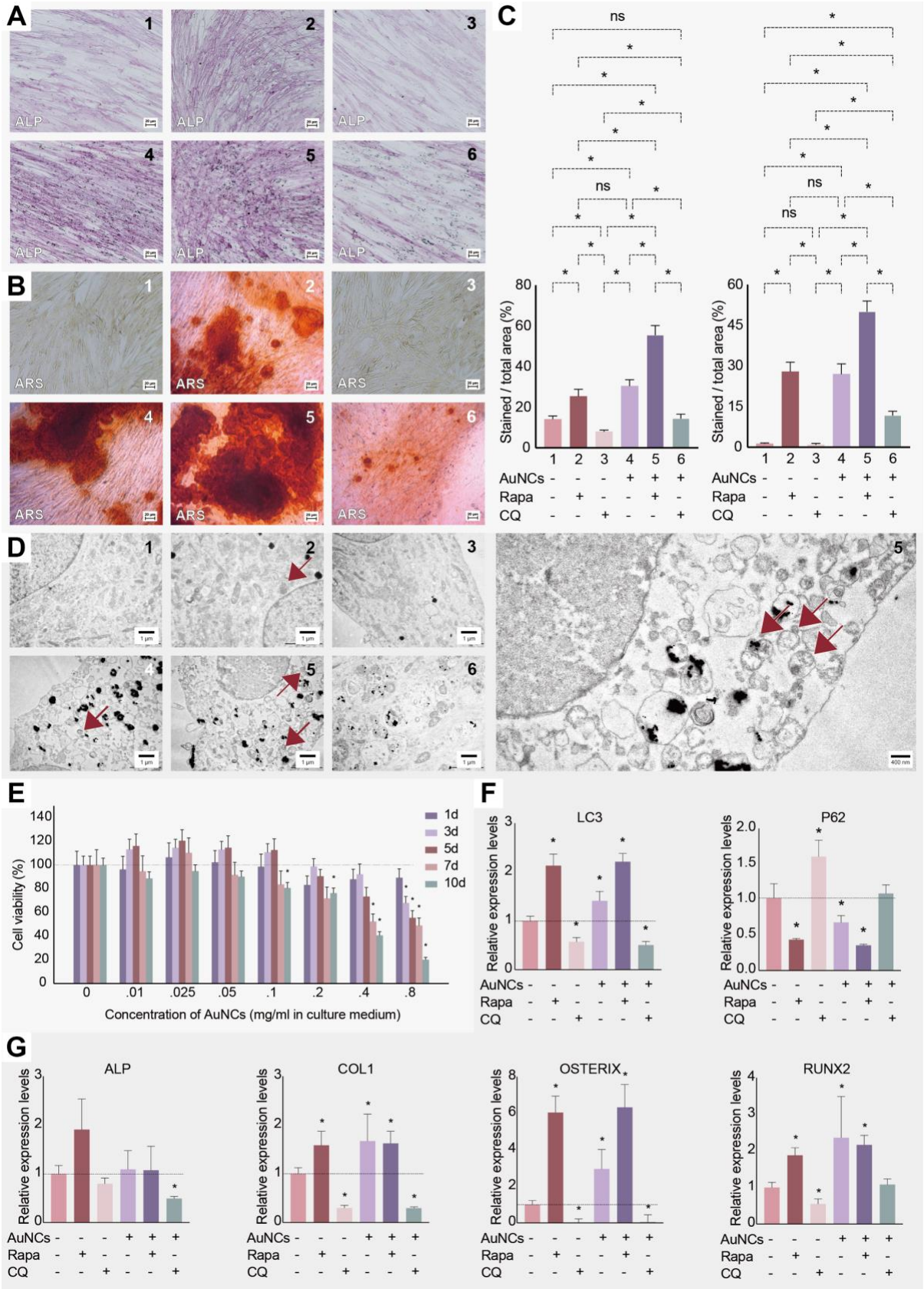

Figure 4. The influence of AuNCs on osteogenic differentiation is associated with autophagy. A, B, C) The ALP and ARS staining show that the autophagy enhancer rapamycin can significantly increase osteogenic functionality ($p < 0.05$). And its effect can be strengthened

when it is applied in combination with AuNCs ($p < 0.05$). In contrast, the autophagy inhibitor chloroquine can significantly reduce osteogenic functionality ($p < 0.05$). The histograms show the quantification of ALP and ARS by ImageJ analysis (n = 6). Scale bar = 20 μm. D) The TEM shows the formation of intracellular autophagosomes, activated by the treatment of rapamycin and/or AuNCs (D2, D4, D5 - magnified on the right side). In contrast, autophagosomes are hardly found in D1, D3 and D6. Scale bar = 1 μm. E) The cell cytotoxicity assay indicates that AuNCs of less than 0.1 mg/mL have no significant cytotoxicity to hPDLSCs even after 7 days of treatment ($p > 0.05$). F, G) The RT-qPCR shows that AuNCs can influence the gene expression of autophagy markers LC3 and P62 ($p < 0.05$). Meanwhile, the autophagy activator and inhibitor can also affect the AuNCs-induced osteogenic differentiation ($p < 0.05$). Data were analyzed with one-way ANOVA and expressed as the mean (n = 6) with SD error bars. *($p < 0.05$) versus hPDLSC cultured in CM without AuNCs, rapamycin, or chloroquine.

2.5. hPDLSCs transplantation does not alter orthodontic tooth movement (OTM)

An animal study was performed on thirty adult male rats to explore the potential effect of AuNC-induced hPDLSCs transplantation on the alveolar bone. Since faster tooth movement is related to increased bone resorption, the acceleration or deceleration of OTM could be linked with bone loss or bone preservation, respectively. Animals were divided into five groups (**Table 2**). Micro-computed tomography (micro-CT) was captured right before (T0) and after 31 days (T1) of force loading on the maxillary first molar.

As shown in **Figure 5**, the analysis of micro-CT imaging showed that all the first molars in Groups 2, 3, 4 and 5 had significant OTM ($p < 0.05$) compared to the control group (Group 1). However, there was no statistically significant difference in OTM between Groups 2, 3, 4 and 5 ($p > 0.05$). The result indicates that either the sham, untreated hPDLSCs or AuNP-induced hPDLSCs transplantation did not influence the OTM of the first molar.

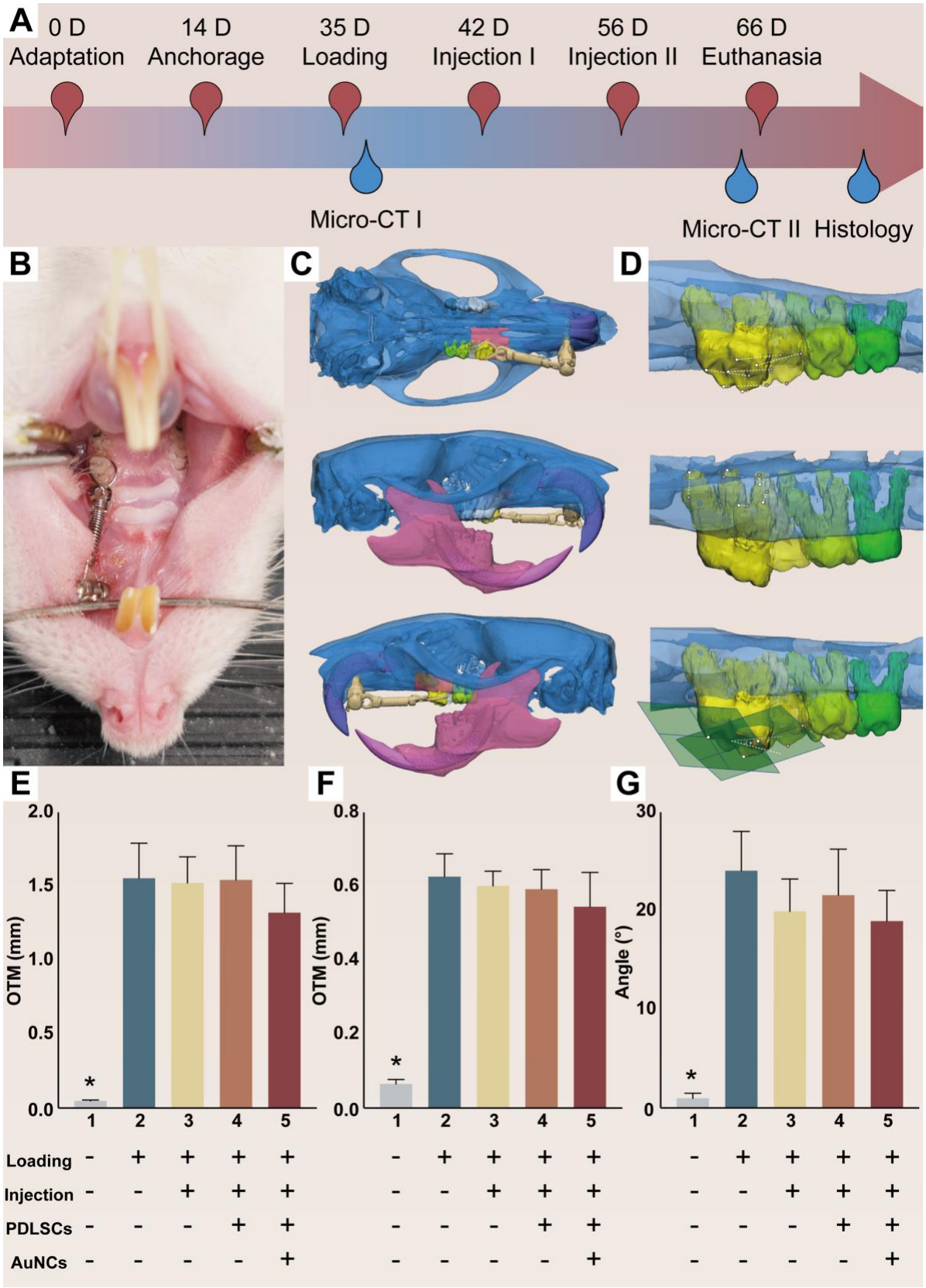

Figure 5. The difference in tooth displacement among groups.

A) Timeline of the animal study. B) The orthodontic force-loading system inducing OTM. C) Relevant structures segmented in 3D for registration and analysis. D) Reference points used to

measure the occlusal, apical and angular movement of the upper first molar. E, F, G) Comparison of the occlusal, apical and angular movement of the maxillary first molar among the five groups, respectively. Data were analyzed with one-way MANOVA and expressed as the mean with SD error bars (n = 6). *$p < 0.05$ versus Group 2.

2.6. AuNCs-induced hPDLSCs transplantation protects alveolar bone from resorption

To further explore whether the transplantation of AuNC-induced hPDLSCs could influence bone regeneration during OTM, the changes in bone morphometry were assessed with micro-CT after the voxel-based registration. Bone mineral density (BMD, g/cm^3), bone volume fraction (BV/TV, %), bone surface density (BS/TV, 1/mm), trabecular number (Tb.N, 1/mm), trabecular thickness (Tb.Th, mm) and trabecular separation (Tb.Sp, mm) were evaluated and compared between the five groups. (**Figure 6**)

Group 1 (negative control) showed no statistically significant change in bone morphometric parameters ($p > 0.05$). In Group 2 (positive control), on the other hand, the BMD, BV/TV, Tb.N diminished significantly when Tb.Th and Tb.Sp increased ($p < 0.05$). Similarly, BMD, BV/TV, Tb.Th, Tb.N and Tb.Sp changed significantly with OTM in Groups 3 and 4 ($p < 0.05$). This demonstrated that neither the injection procedure nor the transplantation of untreated hPDLSCs could prevent the alveolar bone from resorption. Conversely, in Group 5 where AuNC-induced hPDLSCs were transplanted, BMD, BV/TV, Tb.Th, Tb.N had no statistically significant difference compared to the negative control ($p > 0.05$). This implied that the biomimetic periodontal ligament transplantation protected the alveolar bone surrounding the maxillary first molar after protracting it with orthodontic force.

The transplantation of the AuNP-induced hPDLSCs prevented orthodontically induced alveolar bone loss, while sham transplantation and untreated hPDLSCs transplantation did not.

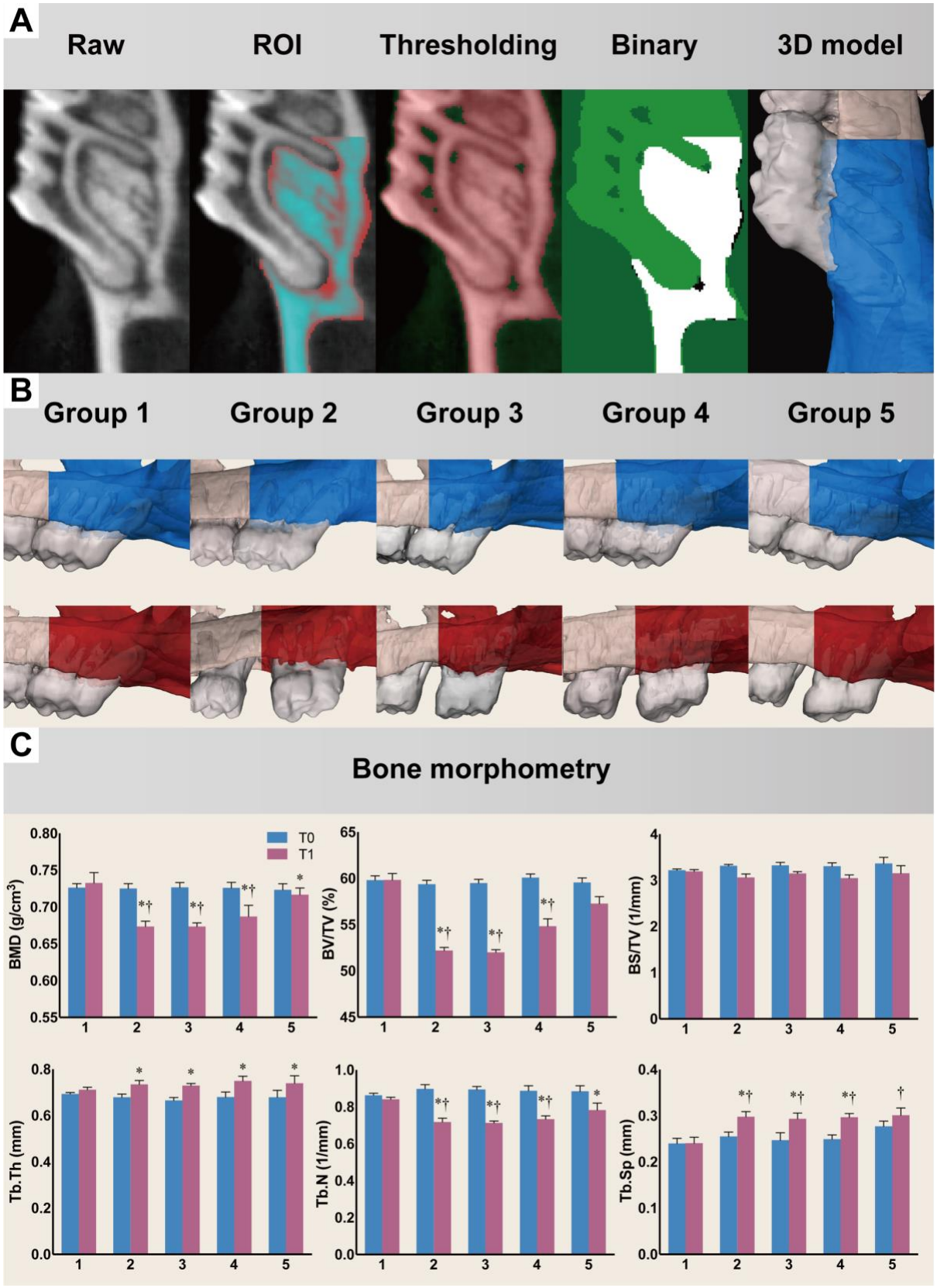

Figure 6. The difference in bone morphometry between groups.

A) The workflow of ROI selection and 3D segmentation for the assessment of bone morphometry. B) 3D changes in bone morphometry from T0 to T1 in different groups. Blue =

T0, Red = T1. C) Comparison of bone morphometry between the five groups. Data were analyzed with two-way repeated measures MANOVA and expressed as the mean with SD error bars (n = 6). *$p < 0.01$ versus Group 1. †$p < 0.01$ versus T0 in the same group.

2.7. Immunohistochemical assay confirms the results of *in vivo* imaging

To verify the changes in bone morphometry among different groups observed by micro-CT imaging, an immunohistochemical (IHC) assay was performed right after the euthanasia of the rats. IF staining of OPG, RANKL, P62, LC3A/3B and Beclin 1 was used to visualize the coupling of bone formation and resorption and the level of autophagy. In addition, Ki67 and Lamin A/C were used to distinguish the transplanted hPDLSCs from the surrounding host tissue.

For Hematoxylin and Eosin staining (H&E staining), Group 1 acted as a baseline, in which few osteoclasts and osteoblasts were detected. This was expected since no orthodontic force was used, and bone homeostasis was intact. However, in Groups 2, 3 and 4, more aggregation of osteoclasts was noticeable in the periodontal ligament and the alveolar bone, where bone resorption was occurring. This was especially prevalent between the loaded maxillary first molar and its adjacent second molar, as indicated by the black arrows in **Figure 7A**. However, in Group 5, the aggregation of osteoclasts was concomitant with that of osteoblasts, often surrounded by a layer of newly-formed osteoid, as indicated by the white arrow.

In the IF staining, the OPG/RANKL ratio was significantly lower in Groups 2, 3 and 4 than in Group 1 ($p < 0.05$), indicating active alveolar bone loss, as shown in **Figure 7B, D**. However, the OPG/RANKL ratio of Group 5 was significantly higher than that of Groups 2, 3 and 4 ($p < 0.05$), and there was no statistically significant difference in OPG/RANKL between Group 1 and 5 ($p > 0.05$). Furthermore, as for the autophagy markers, Group 5 had significantly lower expression of P62, but higher LC3A/3B and Beclin 1, compared to all the other groups ($p < 0.05$), as shown in **Figure 7C, D**. This demonstrated that autophagy was indeed activated in Group 5. There was no significant difference in the expression level of autophagy markers between Groups 1, 2, 3 and 4. Therefore, autophagy was not activated by OTM or injection but by the biomimetic periodontal ligament transplantation of AuNPs-induced hPDLSCs embedded in type-I collagen.

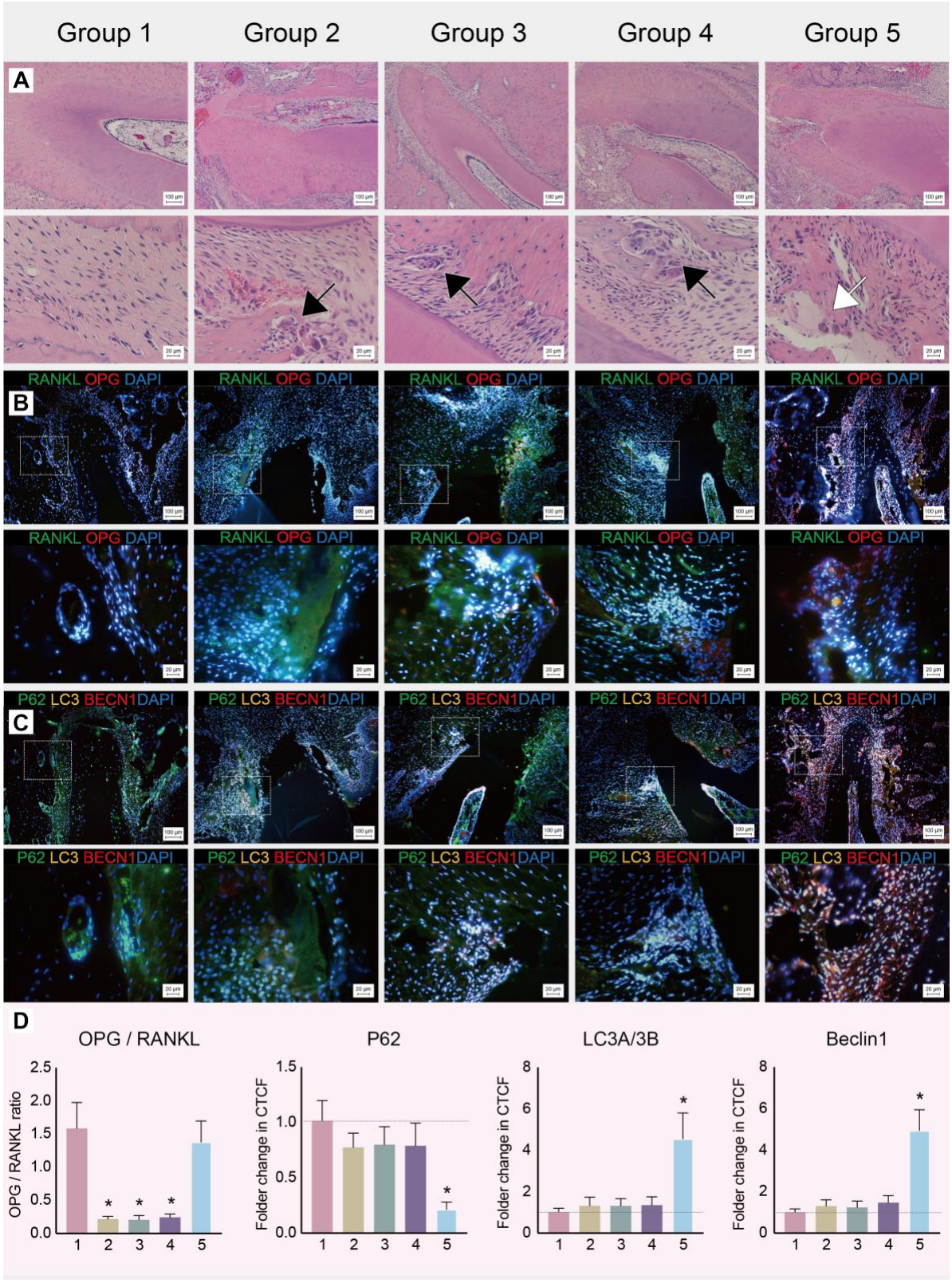

Figure 7. IHC assay of the five groups.

A) H&E staining shows the ROIs of cementum, alveolar bone and periodontal ligament. Black arrows indicate the aggregation of osteoclasts and alveolar bone resorption. The white arrow indicates the transplanted AuNCs-induced hPDLSCs and their surrounding newly-formed

osteoid. B) Overlaid images of the IF staining of osteogenic and osteoclastic markers in the periodontal ligament and alveolar bone shown with 10x and 40x magnification. Blue = DAPI, Green = RANKL, Red = OPG. C) Overlaid images of the IF staining of autophagy markers with 10x and 40x magnification. Blue = DAPI, Green = P62, Orange = LC3A/3B, Red = Beclin 1. D) The histograms show the relative fluorescence intensity measured with ImageJ. All the above data were analyzed with one-way ANOVA and expressed as the mean (n = 6) with SD error bars. *$p < 0.05$ versus Group 1.

3. Discussion

AuNCs have emerged as a promising multimodal material for tissue engineering in regenerative medicine, as they can be easily synthesized, tuned to various sizes and shapes, functionalized, and demonstrate size-dependent optical properties[35, 36]. In addition, AuNCs can also serve as a contrast agent for *in vivo* cell tracking of MSCs[37]. However, their biocompatibility, cytotoxicity[38], and effect on cell proliferation and differentiation[39] remain controversial since they have been shown to promote[25, 36] and not promote[23, 40] proliferation and osteogenic differentiation *in vitro*. These contradictory results might be the result of the differences in size, surface charge, concentration and dose of the applied AuNCs[41]. In the current study, we investigated the effect of optimized AuNCs on PDLSCs as a transplantation pretreatment and conducted a series of *in vitro* experiments to verify these effects and determine the optimal working concentration.

Firstly, the SEM and TEM results demonstrated excellent uptake of AuNCs by hPDLSCs. 40 nm AuNCs at a concentration of 0.1 mg/mL exhibited limited cytotoxicity towards hPDLSCs *in vitro*, and did not have a significant effect on cell proliferation significantly during the first 7 days. After 10 days a slight reduction in cell viability was observed, but this inhibition was much milder than that reported by other research using AuNPs with smaller sizes[42]. A possible explanation may be due to the tendency of ultraminiature AuNCs (diameter $\leq$ 20 nm) to aggregate and enrich in the host cells, resulting in high concentrations of AuNCs inhibiting proper cell functioning.

Secondly, ALP, ARS, IF staining and RT-qPCR demonstrated in multiple levels that 40 nm AuNCs of 0.1 mg/mL can promote osteogenic differentiation of hPDLSCs. This contradicts prior research using AuNCs at 0.05 mg/L where only ALP was selected as the osteogenic marker[23]. In the present study, the selection of multiple osteogenic markers (ALP, COL1,

OSTERIX and RUNX2) and the extended observation period (14 and 21 days) allowed for a more comprehensive evaluation of osteogenic differentiation.

Thirdly, the significant change in the expression of autophagy markers and the massive formation of autophagosomes demonstrate that AuNCs activated autophagy as well. On their own, AuNCs in CM elicited autophagy and osteogenic differentiation. Moreover, when hPDLSCs were cultured in OM, the AuNCs provoked a synergistic effect, resulting in an even more remarkable autophagy and osteogenic differentiation, similar to a previous study[43]. Intriguingly, the gene expression of osteogenic markers was altered when an autophagy activator and inhibitor were applied, suggesting that the activation of autophagy in hPDLSCs might be responsible for the osteogenic differentiation induced by AuNCs, which is consistent with previous studies[44-46].

Following the *in vitro* experiments, the potential of AuNCs-induced hPDLSCs to prevent alveolar bone loss was evaluated *in vivo*. Most previous research in bone regeneration focus on the reconstruction of bone defects rather than on the prevention of bone resorption. In our study, bone regeneration and remodeling are actually investigated through an animal model of OTM. Orthodontic force leads to aseptic inflammation, which induces bone resorption and enables tooth movement. This eliminates the potential bias and confounding factors associated with studying alveolar bone loss induced by infection, trauma, tooth extraction or surgically-inflicted defects. Compared to the previous research based on experimental bone defects or existing alveolar bone atrophy, in the current animal model alveolar bone resorption evolves together with tooth movement. This allowed us to investigate whether biomimetic transplantation could prevent the alveolar bone from resorption, while previous models were only able to evaluate if the transplantation reconstructed a certain alveolar bone defect. This is a valuable asset of the current model, considering the irreversibility of bone resorption. Last but not least, the utilized OTM model is relatively inexpensive and allows for 3D analysis, making it ideal to study bone resorption.

The *in vivo* design also presents several additional advantages. The power of the sample size was calculated at 90%, with the animals being divided into five groups. Groups 1 and 2 were used as the negative and positive control, respectively, while Groups 3 and 4 served to determine possible confounding effects of the scaffold or the PDLSCs injection without AuNCs. Micro-CT images of the same animal were captured at baseline (T0) and after 31 days (T1), allowing longitudinal follow-up. In this way, the effect of transplanted AuNCs-induced hPDLSCs could, respectively, be investigated per group and through time, and the changes in tooth displacement, bone morphometry and periodontium histology could be mutually verified.

The periodontal ligament injection was repeated by 3 times, with an interval of 7 days, to avoid the situation that the scaffold completely degraded and the transplanted cells lost viability during the whole 31-day observation period. While an additional transplant of AuNC without cells was considered as a potential Group 6, this was not included due to the concentration discrepancy caused by AuNC uptake. In Group 5 (AuNCs-treated hPDLSCs), after the 12-hour pretreatment, the AuNCs were no longer in the hydrogel scaffold but had been absorbed by hPDLSCs. The hPDLSCs were subsequently washed with PBS to remove the excessive extracellular AuNCs before being transplanted *in vivo*. The number of intracellular AuNCs in Group 5 would therefore not be comparable to that of Group 6 (0.1 mg/mL in 80 μL hydrogel scaffold). Furthermore, as stated previously, the intervention did not involve the surgical creation of an artificial bone defect to investigate bone regeneration, unlike other studies[47, 48]. In these types of studies, bone regeneration is inevitable following bone resorption, while possible infection and subsequent inflammation from the surgical wound could be confounding factors. In contrast, we performed the transplantation during OTM and not afterward, to explore whether the transplantation could protect the alveolar bone before resorption, which allowed for exploring what occurred during this process. Additionally, since the transplantation was performed with a periodontal ligament injection, no gingival flap or alveolar bone exposure was necessary. Contrasting these invasive procedures, a simple injection would result in minimal inflammation with the added benefit that the periodontal ligament cells possess moderate antimicrobial potential [49]. A final benefit lies in the used type-I collagen hydrogel scaffold. Collagen is the primary component of the periodontal ligament and resembles the native physiological niche of PDLSCs, which greatly facilitates their differentiation into an osteogenic lineage[50].

With these advantages, the *in vivo* model yielded valuable data on OTM and alveolar bone morphometry with or without AuNPs. OTM was unaffected by either sham, untreated or AuNP-induced hPDLSCs transplantation. However, significantly less alveolar bone loss was observed in the group of AuNPs-induced hPDLSCs transplantation, which may have two potential explanations. Firstly, the observation period of 31 days might be insufficient to identify additional significant differences among groups. However, extending the observation period is not possible under the current circumstances. According to the manufacturer, the used coil spring can only deliver a constant orthodontic force of 25 cN when stretched by 9~15 mm. If the observation period was extended longer than 31 days, the coil would have shrunk beyond 9 mm due to the movement of the loaded tooth, resulting in the loss of required constant force. This is one of the reasons why many orthodontic studies in rodents have observation periods

ranging from 2 to 4 weeks. The second explanation may be that the AuNCs-induced hPDLSCs were not able to prevent or inhibit bone resorption but actually promoted bone regeneration simultaneously or even subsequently to bone resorption without affecting the OTM. If this hypothesis is true, Groups 2, 3 and 4 should have areas of lower bone density due to the regeneration not being able to catch up with the movement, whereas group 5, would have stable bone around the moving tooth due to the increased bone regeneration. Unfortunately, this was not investigated as a much larger sample size would have been necessary due to the need for additional timepoints during OTM (not only T0 and T1), making it a more cross-sectional study instead of a longitudinal analysis.

The IHC analysis further confirmed the observed differences among groups. In group 1, the alveolar bone margin was intact and smooth upon H&E staining, whereas in the other four groups, it was serrated and irregular. Moreover, in Groups 2, 3 and 4, plenty of osteoclasts aggregated near the margins of the alveolar bone, particularly between the loaded maxillary first molar and its adjacent second molar. Conversely, the aggregation of osteoclasts was accompanied by newly-formed osteoid in Group 5, exhibiting bone remodeling in the periapical areas. This indicates that despite the applied orthodontic force, the bone remodeling was not dominated by bone loss, but that bone resorption and regeneration were simultaneously activated due to the presence of the AuNCs-induced hPDLSCs. Additionally, IF staining confirmed predominant bone resorption in Groups 2, 3 and 4, as well as bone regeneration in Group 5, with elevated levels of autophagy relative to Group 1. The distinction between Group 5 and the others demonstrates the benefits of *in vivo* application of AuNCs-induced hPDLSCs

Interestingly, although the hPDLSCs were only injected at the cervical level of the first maxillary molar, transplanted hPDLSCs were detected with the IHC analysis in multiple areas, including the periodontal ligament surrounding the apical dental root, the inter radicular area, and even the dental pulp of these teeth (**Supplementary Figure 1**) of these teeth. Immunopositivity for human Ki67, an important cell proliferation marker highly expressed in cycling cells but heavily downregulated in resting G0 cells[51], distinguished the transplanted hPDLSCs from surrounding host cells and confirmed that these cells were actively dividing. Immunopositivity for Lamin A/C, an intermediate filament protein from the nuclear lamina which is fundamental for the migration and differentiation of human MSCs[52], verified the migration of hPDLSCs. This is in line with previous research that suggests an association between orthodontic loading and the reaction of the dental pulp, through increased oxidative stress, pulp sensibility, and decreased pulp blood flow[53, 54]. Future research should investigate

whether the migration of hPDLSCs was coincidental or potentially a pulp-protective mechanism.

4. Conclusion

The current study presents a straightforward method for alveolar bone preservation via biomimetic hPDLSC transplantation. The results demonstrated that pretreatment of hPDLSC with AuNP–Poly-L-lysine hydrobromide–rhodamine B isothiocyanate before transplantation promotes osteogenesis and autophagy. *In vitro*, AuNCs at a concentration of 0.1 mg/mL significantly enhanced the osteogenic differentiation of hPDLSCs *in vitro*, with minimal cytotoxicity. *In vivo*, the biomimetic transplant of AuNCs-induced hPDLSCs was tested in an animal OTM model. The AuNP-pretreated transplant effectively stimulated osteogenesis and prevented alveolar bone resorption without affecting tooth movement. Furthermore, autophagy was investigated and identified as a crucial underlying mechanism in the observed alveolar bone regeneration. The presented results provide compelling evidence for the application of AuNCs as a pretreatment for stem cell therapy and open a new door for addressing the challenge of alveolar bone loss in dentistry.

5. Experimental Section

Materials: Gold nanoparticles (AuNPs) with 40 nm diameter were purchased from British Biocell International (Cardiff, UK). Poly-L-lysine hydrobromide (PLL), paraformaldehyde (PFA), crystal violet, rhodamine B isothiocyanate (RBITC), phosphate-buffered saline (PBS), dimethyl sulphoxide (DMSO), Triton X, Tween 20, sodium phosphate, alizarin red S and monoclonal mouse anti-Lamin A/C antibody were purchased from Sigma-Aldrich (MO, US). Dulbecco's Modified Eagle Medium (DMEM), fetal bovine serum (FBS), bovine serum albumin (BSA), GlutaMax, penicillin-streptomycin, amphotericin B, Trypsin-ethylenediamine tetra-acetic acid (EDTA), polyclonal antibodies for LC3A/LC3B, OPG (also known as TNFRSF11B), Beclin 1, Ki67, monoclonal antibodies for P62 (also known as SQSTM1), RANKL (also known as CD254), CD29, CD45, CD73, CD90 and CD105, secondary antibody Alexa Fluor 488 and 633 were purchased from Thermo Fisher Scientific (MA, US). Cyanine 3 AffiniPure anti-sheep IgG antibody was purchased from Jackson ImmunoResearch (Cambridge, UK). Monoclonal antibodies for CD31, CD34 and CD44 were purchased from ImmunoTools (Friesoythe, DE). AlamarBlue HS Cell Viability Reagent was purchased from Invitrogen (CA, US). Alkaline Phosphatase (ALP) Staining Kit II was purchased from Stemgent (MA, US). StemXVivo Human Osteogenic Supplement was purchased from R&D Systems (MN, US). Rat tail Collagen I HC was purchased from Corning (NY, US). RNAprotect, RNeasy Mini Kit and DNase were purchased from Qiagen (Hilden, Germany). All the information about the antibodies used in this study were shown in **Supplementary Table 1**.

Periodontal ligament cell isolation and characterization: The periodontal ligament samples were collected from the premolars of six healthy young patients (15-20 years old) extracted due to orthodontic reasons. The procedure was performed after approval by the Ethical Commission of KU Leuven and University Hospitals Leuven (S60530) and following informed consent from the donors. Within 20 min after the extraction, the periodontal ligament samples were scraped from the middle 1/3 of the root, and segmented into approximately 1 mm^3 fragments upon which the hPDLSCs were isolated by the outgrowth method[55].
All cells were routinely screened in our lab for the expression of the following markers: CD29, CD31 (negative), CD34 (negative), CD44, CD45 (negative), CD73, CD90, CD105, as described previously[23]. Their MSC properties were investigated by the following experiments:

- Colony-forming unit assay: hPDLSCs of 4×10^3 per well were inoculated in 6-well plates with 2 mL culture medium changed every 2 days. After 3 weeks, the cells were fixed with 4% PFA for 20 min and stained with 1% crystal violet for 1h. The cell colonies consisting of more than 50 cells were observed using light microscopy (Primo Vert, Carl Zeiss, Jena, Germany).
- Cell-doubling time assay: hPDLSCs of 5×10^5 per well were inoculated in T175 culture flasks with 20 mL culture medium changed every 2 days. After 3, 6, 9, and 12 days, the cells were collected and counted to produce a cell-growth curve.
- Cell viability assay: hPDLSCs of 5×10^3 per well were inoculated in 96-well plates with 0.1 mL culture medium changed every 2 days. After 1, 3, 5, and 7 days, the cell viability was longitudinally assessed by AlamarBlue HS Cell Viability Reagent as described before[56].
- Osteogenic differentiation assay: hPDLSCs of 8×10^3 per well were inoculated in 24-well plates with 0.5 mL culture medium. When the cells reached 80% confluence, the medium was replaced by osteogenic medium composed of culture medium and 5% StemXVivo human osteogenic supplement. The osteogenic medium was changed every 2 days. After 3 weeks, the cells were fixed with 4% PFA, upon which the ALP and ARS staining were performed.

hPDLSCs were maintained at 37 °C in a humidified atmosphere containing 5% CO_2, with the culture medium changed every 2–3 days. When the cells reached 80% confluence, they were harvested by 0.25% trypsin-EDTA and were counted as passage 0. All experiments were conducted with hPDLSCs between passages 2 and 6.

AuNCs synthesis and characterization: The AuNCs were prepared as follows: Briefly, 33.3 mL of 40 nm citrate capped AuNP suspension (60 µg/mL, 2 mg in total) was blended with 1.46 mL PLL (1 mg/mL in distilled water) to neutralize the negative surface charge. Second, 2.08 mg of RBITC was added to the AuNP-PLL complexes to render them fluorescent. After removing the excess RBITC, the nanocomplexes were suspended in 20 mL of culture medium (DMEM GlutaMax supplemented with 10% heat-inactivated FBS, 1% penicillin-streptomycin and 1% amphotericin B). The final concentration of AuNCs was 0.1 mg Au/mL.

The spherical morphology and physical diameter of AuNCs in distilled water were confirmed by TEM (JEM-1400Flash, JEOL Ltd., MA, US) and SEM (Nova NanoSEM 450, FEI, US). Two hundred AuNCs were randomly selected during TEM to measure their particle diameter.

Then their size distribution was analyzed by DLS (Litesizer 500, Anton Paar, Graz, AT) with a 40 mW semi-conductor red laser with a wavelength of 658 nm and the preferred measurement angle was automatically selected by the instrument. A volume of 1 ml of the 1 mg/mL AuNCs solution was placed in an Omega cuvette (Anton Paar GmbH). The zeta potential value (ζ, mV) of AuNCs, was determined by ELS(Litesizer 500, Anton Paar). Reported values are an average of hundred runs measured at 25 °C and 37 °C, respectively.

Cell treatment and microscopy: hPDLSCs were seeded on a 24-well culture plate at a density of 3 x 10^4 cells per well. When they reached 80% confluence, the culture medium was replaced by 0.5 mL of culture medium containing 0.1 mg/ml AuNCs. After 12 h, hPDLSCs were fixed for 15 mins with 4% PFA, stained with 1μg/ml DAPI and observed by brightfield and fluorescence microscopy. TEM was used to further confirm the cellular uptake of the AuNCs and to compare the autophagosome between treated and untreated hPDLSCs. Prior to TEM, hPDLSC were cultured on plastic Thermanox coverslips for 3 days and processed as described previously[57].

The surface features of the hPDLSC with or without AuNCs were visualized using SEM with an in-lens secondary electron detector (magnetic immersion lens) for a higher nanoscale resolution. The SEM was operated at a working distance of 5 mm and a low accelerating voltage of 5 keV to increase the surface sensitivity of the imaging and to minimize beam damage on the enzyme coatings. Prior to SEM, a thin platinum layer of approximately 4 nm was sputter-coated on the surface by a turbomolecular pumped coater (Q150T ES plus, Quorum, UK) to improve the conductivity.

Cell cytotoxicity assay: hPDLSCs were seeded into 96-well culture plates at a density of 5 x 10^3 cells per well in 100 μL culture medium. When they reached 80% confluence, the culture medium containing AuNCs was added at different concentrations (0.025, 0.05, 0.1, 0.2 and 0.4 mg Au/mL). 100 μL cell-free culture medium without AuNCs was used as blank control, cells in 100 μL culture medium without AuNCs were used as positive control while cells in 100 μL culture medium with 1% Triton-X were used as a negative control.

The cell cytotoxicity of AuNCs was evaluated by longitudinal tracking of the cell viability with AlamarBlue HS Cell Viability Reagent for 14 days. Briefly, 100 μL 10% AlamarBlue HS Cell Viability Reagent was added to each well and incubated for 4 h at 37 °C on days 1, 3, 5, 7, 10. The fluorescent signal of the supernatant was monitored at 560 nm excitation wavelength and 590 nm emission wavelength. The relative viability was expressed in fluorescence intensity,

calibrated by the average blank control and compared among different samples by repeated measures ANOVA in PRISM 9 (Graphpad, CA, US).

ALP and ARS: To test the effect of AuNCs on the hPDLSCs osteogenic functionality, the cells were cultured in 24-well culture plates and divided into four different groups, treated with or without AuNCs (0.1 mg Au/mL) in CM or OM. Autophagy inhibitor chloroquine (0.5 μM) and autophagy enhancer rapamycin (4 μM) were used to further test the role of autophagy in osteogenic functionality.

The medium was changed every 2 or 3 days. After 21 days, the cell layer was fixed in 4% PFA for 20 min at room temperature. The hPDLSCs incubated in CM and fixed after 5 days were used as a negative control. The ALP activity was evaluated with ALP Staining Kit II according to the manufacturer's instructions. In addition, the mineralized nodule formation was evaluated with ARS staining.

The ALP and ARS staining of cells in different groups was quantified with ImageJ (version 1.5.3, NIH, US) and compared by one-way ANOVA in PRISM 9.

RT-qPCR: To test the effect of AuNCs on the gene expression of osteogenic markers, hPDLSCs treated with or without AuNCs (0.1 mg Au/mL) were cultured in 24-well culture plates for 14 days with CM or OM. To investigate the role of autophagy in AuNCs-induced cell osteogenic differentiation, chloroquine (0.5 μM) and rapamycin (4 μM) were also introduced in hPDLSCs, as shown in **Table 1**.

Table 1. Groups of different cell treatments for RT-qPCR gene expression analysis

Treatment	Group							
	1	2	3	4	5	6	7	8
AuNCs(0.1 mg Au/mL)	−	−	−	−	+	+	+	+
Rapamycin(4 μM)	−	+	−	−	−	+	−	−
Chloroquine(0.5 μM)	−	−	+	−	−	−	+	−
Osteogenic induction	−	−	−	+	−	−	−	+

After 14 days, total RNA was extracted from the cells using RNAprotect and RNeasy mini kit. Genomic DNA was removed with DNase during the extraction. After the extraction, RNA quality and quantity were measured using a SimpliNano spectrophotometer (Biochrom,

Cambridge, UK) and the samples were diluted with RNase-free water to match the lowest concentration. cDNA was synthesized using the PrimeScript 1st strand cDNA synthesis kit with random hexamers (Takara Bio, Shiga, Japan). Gene expression was quantitatively analyzed by mixing 12.5 µL Takyon Rox SYBR master mix dTTP blue (Eurogentec, Seraing, Belgium), 1 µL of each primer at a final concentration of 300 µM, 4.5 µL water, and 5 µL template. RT-qPCR was performed in a CFX96 real-time PCR detection system (Bio-Rad, CA, USA) with cycle conditions: initial step at 50 °C for 2 min and 95 °C for 10 min, followed by 45 cycles of 95 °C for 15 s and 60 °C for 1 min. The relative expression levels of osteogenic markers (ALP, COL1, OSTERIX and RUNX2) and autophagy markers (LC3 and P62) were evaluated with GAPDH as a reference gene[58]. Statistical analysis was performed on the ΔCq values and presented as fold change in expression ($2^{-\Delta\Delta Cq}$) according to Livak *et al.* (2001) [59]. The primers (IDT, Haasrode, Belgium) in **Supplementary Table 2** were used for the analysis.

Scaffold preparation of type-I collagen hydrogel: The collagen hydrogel scaffold was prepared as described previously[60]. Briefly, the acid-solubilized rat type-I collagen at a concentration of 9.0 mg/ml was used. The collagen hydrogel was fabricated by combining acidic collagen with a concentrated buffer (10X DMEM, no supplement), neutralization agent (1N NaOH), and physiological buffer (1X DMEM GlutaMax supplemented with heat-inactivated FBS, penicillin-streptomycin and amphotericin B). The volume fraction of each component was calculated as follows: type-I collagen = 0.5, 10X DMEM = 0.1, NaOH=0.015, 1X DMEM = 0.385. Hereby, the pH was adjusted to 7.4 ± 0.1 and the solution was diluted with PBS to reach a final collagen concentration of 4.5 mg/ml.

Interventions in the animal model: Thirty young adult male Wistar rats (9 weeks old) were included in this study. The sample size was calculated using a previous split-mouth study[33]. A power analysis in the software G*Power 3.1 (Düsseldorf, Germany) suggested a total sample size of minimum thirty animals for ANOVA when assuming 90% power with $\alpha = 0.05$.
The rats were divided into five groups as shown in **Table 2**. **Group 1**: a self-drilling mini-screw (2.5 × 1.3 × 5 mm, DEWIMED, Tuttlingen, Germany) was implanted approximately 2 mm distal to the upper incisors with an angulation of 45° to the occlusal plane, but no orthodontic tooth movement (OTM) was induced. **Group 2**: The mini-screw was implanted in the same way as in Group 1 and was used as skeletal anchorage to protract the rats' upper molars. After 3 weeks of healing time to ensure stability, OTM was induced by applying a

constant orthodontic force of 25 cN on one hemimaxilla. The force loaded between the mini-screw and the maxillary first molar was provided by a Sentalloy closed coil spring (Ultra-light, Dentsply GAC, Rochecorbon, France)[61]. No orthodontic force was loaded on the contralateral hemi-maxilla. **Group 3**: Orthodontic force was loaded in the same way as in Group 2. In addition, 80 μL type-I collagen hydrogel scaffold (9.1 mg/ml) was injected around the loaded first molar via periodontal ligament injection at days 7, 14 and 21 during OTM. This was considered a sham transplantation. **Group 4**: Orthodontic force was loaded in the same way as in Groups 2 and 3. Additionally, hPDLSCs embedded in 80 μL type-I collagen hydrogel scaffold (5×10^6 cells/ml) were transplanted around the loaded maxillary first molar via periodontal ligament injection at days 7, 14 and 21 during OTM. **Group 5**: Orthodontic force was loaded in the same way as in Groups 2, 3 and 4. Additionally, hPDLSCs treated with AuNCs (0.1 mg/ml) *in vitro* for 1 day and embedded in 80 μL type-I collagen hydrogel scaffold (5×10^6 cells/ml) were transplanted via periodontal ligament injection around the loaded teeth at days 7, 14 and 21 during OTM.

The animals were housed in ten cages under constant temperature (23 °C), a regular 12-h shift of light-dark cycle, and a standard rat maintenance diet. Weekly surveillance was performed in order to track weight change, guarantee intraoral hygiene and prevent unnecessary animal suffering. All interventions were conducted by the same investigator, firstly under sedation of 2.5–5% isoflurane (1000 mg/g, Iso-Vet, Dechra, Skipton, UK), followed by intraperitoneal anesthesia of 100 mg/ml ketamine (80 mg/kg, Nimatek, Bladel, Netherlands) and 2% xylazine (10 mg/kg, XYL-M, V.M.D, Arendonk, Belgium). After the interventions, a soft diet and analgesic medication (0.05 mg/kg Buprenorphine) were supplied for 3 days After 31 days of OTM, all the rats were euthanized under anesthesia. All animal experiments were performed in the Laboratory Animal Center and the Molecular Small Animal Imaging Center (MoSAIC) of KU Leuven, Belgium, with the approval of KU Leuven Ethical Committee for Animal Experimentation (P197/2019) and in accordance with the EU Directive 2010/63/EU and ARRIVE 2.0. Guidelines.

Table 2 Groups of different treatments for the animal study.

Group	Animal number	Treatment
1	6	No OTM
2	6	OTM
3	6	OTM + sham transplantation
4	6	OTM + hPDLSCs transplantation
5	6	OTM + AuNCs-treated hPDLSCs transplantation

In vivo Micro-CT: The animals were longitudinally followed up with micro-CT right before (T0) and after 31 days of OTM (T1). The image acquisition was performed by a non-destructive, high-resolution *in vivo* micro-CT (Skyscan 1278, Bruker, Kontich, Belgium) following an optimized scan protocol at 65 kVp, 500 μA, and 180° with an angular rotation step of 0.5°, resulting in an exposure time of 50 ms. A 1 mm aluminum filter was used to eliminate the beam hardening effect. Flat field correction was performed before the actual image acquisition for a calibration based on the empty field of view. Animals were sedated with 2.5–5% isoflurane during image acquisition. After image acquisition, the image stacks were reconstructed with NRecon software (version 1.7.1, Bruker, Kontich, Belgium). Correction for post-alignment and ring-artifacts reduction were optimized per scan if needed. Smoothing level and beam hardening were applied with 0 and 10% values, respectively. The dynamic image range of the histogram was set from 0.003 to 0.03.

Assessment of OTM and bone morphometry: The tooth movement of the maxillary first molar and changes in bone morphometry were evaluated by a rigid voxel-based registration method as described previously[33, 61]. Firstly, the CT data captured at T1 were superimposed with the corresponding baseline scan at T0 based on the maxillary structures as a reference in MTM Scaffold Strain (KU Leuven, Leuven, Belgium). Second, the teeth and their surrounding alveolar bone at both T0 and T1 were delineated by the same investigator as a region of interest (ROI) in CTAnalyser software (version 1.17.5, Bruker, Kontich, Belgium). The ROIs were segmented using an adaptive threshold algorithm[62] as individual 3D standard tessellation language (.STL) models. The stl models were loaded in 3-Matic (version 17.0, Materialise, Leuven, Belgium) to assess OTM and bone morphometry.

To assess the OTM of the maxillary first molar, six reference points on the cusps and five on the root apices were created. Their displacement between T0 and T1 was defined as occlusal and apical movement, respectively. The angular change in the occlusal plane determined by

three reference points on the cusps was defined as the angular movement. The occlusal, apical and angular movements among the five groups were compared to investigate the effect of hPDLSCs transplantation on OTM.

To assess the bone morphometry, bone mineral density (BMD, g/cm^3), bone volume fraction (BV/TV, %), bone surface density (BS/TV, mm^{-1}), trabecular number (Tb.N, mm^{-1}), trabecular thickness (Tb.Th, mm) and trabecular separation (Tb.Sp, mm) were evaluated as described by Chatterjee *et al.* (2017) [63] and compared among the five groups.

IHC analysis: To further explore the effect of the transplanted hPDLSCs in rats, a series of IHC assays were performed.

First, the hemi-maxilla of the orthodontic force side was dissected from the skull immediately after euthanasia. The sample of the maxillary first molar, its periodontal ligament and surrounding alveolar bone were isolated from the hemi-maxilla. Each sample was fixed with 4% PFA for 48 h, dehydrated, and embedded into paraffin blocks. The blocks were trimmed and cut in 5 μm sections using a rotary microtome (HM340E, Thermo Fisher Scientific). The sections were mounted on coated Flex IHC microscope slides (K802021-2, Dako) and dried overnight at 55°C. Automated deparaffinization of the tissue sections was performed in the Leica Autostainer XL (ST5010, Leica, Diegem, Belgium). Next, epitopes were retrieved by heat-induced epitope retrieval using citrate buffer (pH = 6) for 10 min at 97°C in a PT Link module (Dako).

Second, H&E staining was used to identify representative sections which could simultaneously exhibit the sagittal cross-section of the apical root, periodontal ligament and surrounding alveolar bone of the maxillary first molar. Next, IF staining was performed to visualize the expression of OPG, RANKL, LC3A/3B, Beclin 1, P62, Ki67 and Lamin A/C in samples from different groups. Before IF staining, DAB staining was used to test the validity and proper working concentration of the primary antibodies against the above markers. Briefly, the slides were incubated overnight with mouse anti-P62, anti-RANKL and anti-Lamin A/C antibodies, rabbit anti-LC3A/3B, anti-OPG and anti-Ki67 antibodies and sheep anti-Beclin 1 antibody (primary antibodies), in a humid chamber at room temperature. The primary antibodies were localized with DAB as substrate and hematoxylin as counterstain. For IF staining, the representative sections were incubated with primary antibodies as described above, washed three times and then incubated with a secondary antibody cocktail consisting of goat anti-mouse AF488, goat anti-rabbit AF633 and donkey anti-sheep Cy3. Subsequently, the slides were mounted with ProLong Gold mounting medium containing DAPI. Finally, the IF staining

was imaged by fluorescence microscopy (LEICA, Wetzlar, Germany). Tissue sections stained only by secondary antibodies but not primary antibodies were used as a blank control.

Statistical analysis: All data were presented as mean ± SD. Statistical analysis was performed using GraphPad Prism software (CA, US). The quantification of ALP and ARS was normally distributed and compared by one-way ANOVA (n = 6). The relative expression levels of osteogenic and autophagy markers were normally distributed and compared by one-way ANOVA (n = 6). The cell viability data were normally distributed and analyzed by two-way repeated measures ANOVA (n = 6). The occlusal, apical and angular movements of the upper first molar were normally distributed and analyzed by one-way ANOVA (n = 6). The bone morphometric data were normally distributed and analyzed by two-way repeated measures ANOVA (n = 6). The fluorescence intensity in the IHC assay was normally distributed and analyzed by one-way ANOVA (n = 6). For all statistical analyses, significance was accepted at the 95% confidence level, and all analyses were two-tailed. Statistical differences with $p<0.05$ were considered significant.

Supporting Information

Supporting Information is available from the Wiley Online Library or the author.

Acknowledgments

Chen Zong was supported by the China Scholarship Council (File No. 201806270252). Maria Cadenas was supported by the 'Start-up Grant for ZAP' of KU Leuven (EGW-D4244-BLOZ/17/014). We would like to thank Stevan Cokic and Mariano Simón Pedano De Piero for their valuable help during the experiments, and Martine Pauwels, Ben Mercelis, Kathleen Van den Eynde, and Eef Allegaert for their excellent technical assistance. The authors are also thankful to KU Leuven institutions, facilities and research groups, including Biomaterials (BIOMAT) and Periodontology & Oral Microbiology (P&OM) of the KU Leuven Department of Oral Health Sciences, the UZ Leuven Medical Department Oral and Maxillo-facial Surgery, and the KU Leuven Department of Imaging & Pathology and Department of Materials Engineering (MTM) for the generous facility support. Rats were obtained from Charles River Laboratories and cared for in the Animal search Center (Biomedical Sciences Group) and Molecular Small Animal Imaging Center.

Conflict of Interest

The authors declare no conflict of interest.

References

[1] G. Avila-Ortiz, S. Elangovan, K. W. Kramer, D. Blanchette and D. V. Dawson. Effect of alveolar ridge preservation after tooth extraction: a systematic review and meta-analysis. J Dent Res. **2014**;93(10):950.

[2] D. Hollý, M. Klein, M. Mazreku, R. Zamborský, Š. Polák, Ľ. Danišovič and M. Csöbönyeiová. Stem Cells and Their Derivatives-Implications for Alveolar Bone Regeneration: A Comprehensive Review. Int J Mol Sci. **2021**;22(21).

[3] M. Timaner, K. K. Tsai and Y. Shaked. The multifaceted role of mesenchymal stem cells in cancer. Seminars in cancer biology. **2020**;60:225.

[4] D. M. Hoang, P. T. Pham, T. Q. Bach, A. T. L. Ngo, Q. T. Nguyen, T. T. K. Phan, G. H. Nguyen, P. T. T. Le, V. T. Hoang, N. R. Forsyth, M. Heke and L. T. Nguyen. Stem cell-based therapy for human diseases. Signal Transduct Target Ther. **2022**;7(1):272.

[5] X. Wang. Stem cells in tissues, organoids, and cancers. Cell Mol Life Sci. **2019**;76(20):4043.

[6] P.-F. Wong, M. D. Devi and T. S. Ramasamy. Senotherapeutics for mesenchymal stem cell senescence and rejuvenation. Drug Discovery Today. **2022**:103424.

[7] R. M. Samsonraj, M. Raghunath, V. Nurcombe, J. H. Hui, A. J. van Wijnen and S. M. Cool. Concise Review: Multifaceted Characterization of Human Mesenchymal Stem Cells for Use in Regenerative Medicine. Stem cells translational medicine. **2017**;6(12):2173.

[8] M. B. Heydari, Z. Ghanbari-Movahed, M. Heydari and M. H. Farzaei. In vitro study of the mesenchymal stem cells-conditional media role in skin wound healing process: A systematic review. Int Wound J. **2022**.

[9] D. Gupta, A. M. Zickler and S. El Andaloussi. Dosing extracellular vesicles. Adv Drug Deliv Rev. **2021**;178:113961.

[10] H. S. Joo, J. H. Suh, H. J. Lee, E. S. Bang and J. M. Lee. Current Knowledge and Future Perspectives on Mesenchymal Stem Cell-Derived Exosomes as a New Therapeutic Agent. Int J Mol Sci. **2020**;21(3).

[11] H. Lin, J. Sohn, H. Shen, M. T. Langhans and R. S. Tuan. Bone marrow mesenchymal stem cells: Aging and tissue engineering applications to enhance bone healing. Biomaterials. **2019**;203.

[12] L. A. Costa, N. Eiro, M. Fraile, L. O. Gonzalez, J. Saá, P. Garcia-Portabella, B. Vega, J. Schneider and F. J. Vizoso. Functional heterogeneity of mesenchymal stem cells from natural

niches to culture conditions: implications for further clinical uses. Cell Mol Life Sci. **2021**;78(2):447.

[13] E. J. Calabrese. Human periodontal ligament stem cells and hormesis: Enhancing cell renewal and cell differentiation. Pharmacol Res. **2021**;173:105914.

[14] J. Botelho, M. A. Cavacas, V. Machado and J. J. Mendes. Dental stem cells: recent progresses in tissue engineering and regenerative medicine. Ann Med. **2017**;49(8):644.

[15] J. Nuñez, F. Vignoletti, R. G. Caffesse and M. Sanz. Cellular therapy in periodontal regeneration. Periodontol 2000. **2019**;79(1):107.

[16] J. Chen, Q. Mo, R. Sheng, A. Zhu, C. Ling, Y. Luo, A. Zhang, Z. Chen, Q. Yao, Z. Cai and W. Zhang. The application of human periodontal ligament stem cells and biomimetic silk scaffold for in situ tendon regeneration. Stem Cell Research & Therapy. **2021**;12(1):596.

[17] F. Mohebichamkhorami, R. Fattahi, Z. Niknam, M. Aliashrafi, S. Khakpour Naeimi, S. Gilanchi and H. Zali. Periodontal ligament stem cells as a promising therapeutic target for neural damage. Stem Cell Research & Therapy. **2022**;13(1):273.

[18] A. Aierken, B. Li, P. Liu, X. Cheng, Z. Kou, N. Tan, M. Zhang, S. Yu, Q. Shen, X. Du, B. B. Enkhbaatar, J. Zhang, R. Zhang, X. Wu, R. Wang, X. He, N. Li, S. Peng, W. Jia, C. Wang and J. Hua. Melatonin treatment improves human umbilical cord mesenchymal stem cell therapy in a mouse model of type II diabetes mellitus via the PI3K/AKT signaling pathway. Stem Cell Research & Therapy. **2022**;13(1):164.

[19] C.-C. Yang, P.-H. Sung, K.-H. Chen, H.-T. Chai, J. Y. Chiang, S.-F. Ko, F.-Y. Lee and H.-K. Yip. Valsartan- and melatonin-supported adipose-derived mesenchymal stem cells preserve renal function in chronic kidney disease rat through upregulation of prion protein participated in promoting PI3K-Akt-mTOR signaling and cell proliferation. Biomed Pharmacother. **2022**;146:112551.

[20] X. Qiu, J. Liu, C. Zheng, Y. Su, L. Bao, B. Zhu, S. Liu, L. Wang, X. Wang, Y. Wang, W. Zhao, J. Zhou, Z. Deng, S. Liu and Y. Jin. Exosomes released from educated mesenchymal stem cells accelerate cutaneous wound healing via promoting angiogenesis. Cell Prolif. **2020**;53(8):e12830.

[21] J. Cheng, X. Ruan, Y. Li, J. Du, F. Jin, M. Gu, Q. Zhou, X. Xu, Y. Yang, H. Wang and A. O. Mueck. Effects of hypoxia-preconditioned HucMSCs on neovascularization and follicle survival in frozen/thawed human ovarian cortex transplanted to immunodeficient mice. Stem Cell Research & Therapy. **2022**;13(1):474.

[22] M. Alfaifi, Y. W. Eom, P. N. Newsome and S. K. Baik. Mesenchymal stromal cell therapy for liver diseases. J Hepatol. **2018**;68(6):1272.

[23] C. Zong, A. Bronckaers, G. Vande Velde, G. Willems and M. Cadenas de Llano-Pérula. In Vivo Micro-Computerized Tomography Tracking of Human Periodontal Ligament Stem Cells Labeled with Gold Nanocomplexes. Adv Healthc Mater. **2022**;11(1):e2101133.
[24] V. di Giacomo, A. Cataldi and S. Sancilio. Biological Factors, Metals, and Biomaterials Regulating Osteogenesis through Autophagy. Int J Mol Sci. **2020**;21(8).
[25] Y. Zhang, N. Kong, Y. Zhang, W. Yang and F. Yan. Size-dependent Effects of Gold Nanoparticles on Osteogenic Differentiation of Human Periodontal Ligament Progenitor Cells. Theranostics. **2017**;7(5):1214.
[26] Y. Yin, B.-M. Tian, X. Li, Y.-C. Yu, D.-K. Deng, L.-J. Sun, H.-L. Qu, R.-X. Wu, X.-Y. Xu, H.-H. Sun, Y. An, X.-T. He and F.-M. Chen. Gold nanoparticles targeting the autophagy-lysosome system to combat the inflammation-compromised osteogenic potential of periodontal ligament stem cells: From mechanism to therapy. Biomaterials. **2022**;288:121743.
[27] X.-D. Chen, J.-L. Tan, Y. Feng, L.-J. Huang, M. Zhang and B. Cheng. Autophagy in fate determination of mesenchymal stem cells and bone remodeling. World Journal of Stem Cells. **2020**;12(8):776.
[28] S. Ceccariglia, A. Cargnoni, A. R. Silini and O. Parolini. Autophagy: a potential key contributor to the therapeutic action of mesenchymal stem cells. Autophagy. **2020**;16(1):28.
[29] X. Chen, H. Fan, X. Deng, L. Wu, T. Yi, L. Gu, C. Zhou, Y. Fan and X. Zhang. Scaffold Structural Microenvironmental Cues to Guide Tissue Regeneration in Bone Tissue Applications. Nanomaterials (Basel). **2018**;8(11).
[30] Q. Ding, J. Cui, H. Shen, C. He, X. Wang, S. G. F. Shen and K. Lin. Advances of nanomaterial applications in oral and maxillofacial tissue regeneration and disease treatment. Wiley Interdiscip Rev Nanomed Nanobiotechnol. **2020**:e1669.
[31] P. K. Raghav, Z. Mann, S. Ahlawat and S. Mohanty. Mesenchymal stem cell-based nanoparticles and scaffolds in regenerative medicine. Eur J Pharmacol. **2022**;918:174657.
[32] I. M. Zurina, V. S. Presniakova, D. V. Butnaru, A. A. Svistunov, P. S. Timashev and Y. A. Rochev. Tissue engineering using a combined cell sheet technology and scaffolding approach. Acta Biomater. **2020**;113:63.
[33] C. Zong, J. Van Dessel, G. Vande Velde, G. Willems and M. Cadenas de Llano-Pérula. Dynamic changes in tooth displacement and bone morphometry induced by orthodontic force. Sci Rep. **2022**;12(1):13672.
[34] M. Dominici, K. Le Blanc, I. Mueller, I. Slaper-Cortenbach, F. Marini, D. Krause, R. Deans, A. Keating, D. Prockop and E. Horwitz. Minimal criteria for defining multipotent

mesenchymal stromal cells. The International Society for Cellular Therapy position statement. Cytotherapy. **2006**;8(4):315.

[35] R. Chandrasekaran, T. Madheswaran, N. Tharmalingam, R. J. Bose, H. Park and D. H. Ha. Labeling and tracking cells with gold nanoparticles. Drug Discov Today. **2021**;26(1):94.

[36] M. Yadid, R. Feiner and T. Dvir. Gold Nanoparticle-Integrated Scaffolds for Tissue Engineering and Regenerative Medicine. Nano Lett. **2019**;19(4):2198.

[37] T. Kim, N. Lee, D. R. Arifin, I. Shats, M. Janowski, P. Walczak, T. Hyeon and J. W. M. Bulte. In Vivo Micro-CT Imaging of Human Mesenchymal Stem Cells Labeled with Gold-Poly-L-Lysine Nanocomplexes. Adv Funct Mater. **2017**;27(3).

[38] M. Kus-Liśkiewicz, P. Fickers and I. Ben Tahar. Biocompatibility and Cytotoxicity of Gold Nanoparticles: Recent Advances in Methodologies and Regulations. Int J Mol Sci. **2021**;22(20).

[39] A. Gupta and S. Singh. Multimodal Potentials of Gold Nanoparticles for Bone Tissue Engineering and Regenerative Medicine: Avenues and Prospects. Small. **2022**;18(29):e2201462.

[40] H.-M. Lo, M.-C. Ma, J.-M. Shieh, H.-L. Chen and W.-B. Wu. Naked physically synthesized gold nanoparticles affect migration, mitochondrial activity, and proliferation of vascular smooth muscle cells. Int J Nanomedicine. **2018**;13:3163.

[41] R. A. Bapat, T. V. Chaubal, S. Dharmadhikari, A. M. Abdulla, P. Bapat, A. Alexander, S. K. Dubey and P. Kesharwani. Recent advances of gold nanoparticles as biomaterial in dentistry. International journal of pharmaceutics. **2020**;586:119596.

[42] Q. Xia, J. Huang, Q. Feng, X. Chen, X. Liu, X. Li, T. Zhang, S. Xiao, H. Li, Z. Zhong and K. Xiao. Size- and cell type-dependent cellular uptake, cytotoxicity and in vivo distribution of gold nanoparticles. Int J Nanomedicine. **2019**;14:6957.

[43] C. Vidoni, A. Ferraresi, E. Secomandi, L. Vallino, C. Gardin, B. Zavan, C. Mortellaro and C. Isidoro. Autophagy drives osteogenic differentiation of human gingival mesenchymal stem cells. Cell Commun Signal. **2019**;17(1):98.

[44] Y. Yang, Y. Sun, W.-W. Mao, H. Zhang, B. Ni and L. Jiang. Oxidative stress induces downregulation of TP53INP2 and suppresses osteogenic differentiation of BMSCs during osteoporosis through the autophagy degradation pathway. Free Radic Biol Med. **2021**;166:226.

[45] L. Huang, X. Yin, J. Chen, R. Liu, X. Xiao, Z. Hu, Y. He and S. Zou. Lithium chloride promotes osteogenesis and suppresses apoptosis during orthodontic tooth movement in osteoporotic model via regulating autophagy. Bioact Mater. **2021**;6(10):3074.

[46] Y. Zhang, P. Wang, Y. Wang, J. Li, D. Qiao, R. Chen, W. Yang and F. Yan. Gold Nanoparticles Promote the Bone Regeneration of Periodontal Ligament Stem Cell Sheets Through Activation of Autophagy. Int J Nanomedicine. **2021**;16:61.

[47] S. Zhang, H. Zhou, N. Kong, Z. Wang, H. Fu, Y. Zhang, Y. Xiao, W. Yang and F. Yan. l-cysteine-modified chiral gold nanoparticles promote periodontal tissue regeneration. Bioact Mater. **2021**;6(10):3288.

[48] Y. Klein, O. Fleissig, A. Stabholz, S. Chaushu and D. Polak. Bone regeneration with bovine bone impairs orthodontic tooth movement despite proper osseous wound healing in a novel mouse model. Journal of Periodontology. **2019**;90(2):189.

[49] E. Könönen, M. Gursoy and U. K. Gursoy. Periodontitis: A Multifaceted Disease of Tooth-Supporting Tissues. J Clin Med. **2019**;8(8).

[50] V. Bunpetch, Z.-Y. Zhang, X. Zhang, S. Han, P. Zongyou, H. Wu and O. Hong-Wei. Strategies for MSC expansion and MSC-based microtissue for bone regeneration. Biomaterials. **2019**;196:67.

[51] X. Sun and P. D. Kaufman. Ki-67: more than a proliferation marker. Chromosoma. **2018**;127(2):175.

[52] N. Alcorta-Sevillano, I. Macías, C. I. Rodríguez and A. Infante. Crucial Role of Lamin A/C in the Migration and Differentiation of MSCs in Bone. Cells. **2020**;9(6).

[53] A. Morii, Y. Miyamura, M. I. Sago, M. Mizuhara, T. Shikayama, M. Naniwa, S. Hitomi, I. Ujihara, K. N. Kuroishi, K. K. Gunjigake, M. Shiga, Y. Morimoto, T. Kawamoto and K. Ono. Orthodontic force-induced oxidative stress in the periodontal tissue and dental pulp elicits nociception via activation/sensitization of TRPA1 on nociceptive fibers. Free Radic Biol Med. **2020**;147:175.

[54] F. C. Vitali, I. V. Cardoso, F. W. Mello, C. Flores-Mir, A. C. Andrada, K. L. Dutra-Horstmann and T. M. Duque. Association between Orthodontic Force and Dental Pulp Changes: A Systematic Review of Clinical and Radiographic Outcomes. J Endod. **2022**;48(3):298.

[55] R. Shinagawa-Ohama, M. Mochizuki, Y. Tamaki, N. Suda and T. Nakahara. Heterogeneous Human Periodontal Ligament-Committed Progenitor and Stem Cell Populations Exhibit a Unique Cementogenic Property Under In Vitro and In Vivo Conditions. Stem cells and development. **2017**;26(9):632.

[56] L. Ortega-Llamas, M. I. Quiñones-Vico, M. García-Valdivia, A. Fernández-González, A. Ubago-Rodríguez, R. Sanabria-de la Torre and S. Arias-Santiago. Cytotoxicity and Wound

Closure Evaluation in Skin Cell Lines after Treatment with Common Antiseptics for Clinical Use. Cells. **2022**;11(9).

[57] W. Martens, K. Sanen, M. Georgiou, T. Struys, A. Bronckaers, M. Ameloot, J. Phillips and I. Lambrichts. Human dental pulp stem cells can differentiate into Schwann cells and promote and guide neurite outgrowth in an aligned tissue-engineered collagen construct in vitro. FASEB J. **2014**;28(4):1634.

[58] N. Celik, M. H. Kim, D. J. Hayes and I. T. Ozbolat. miRNA induced co-differentiation and cross-talk of adipose tissue-derived progenitor cells for 3D heterotypic pre-vascularized bone formation. Biofabrication. **2021**;13(4).

[59] J. L. Kenneth and D. S. Thomas. Analysis of Relative Gene Expression Data Using Real-Time Quantitative PCR and the 2−ΔΔCT Method. Methods. **2001**;25(4):402.

[60] L. M. Dedroog, O. Deschaume, C. J. G. Abrego, E. Koos, Y. de Coene, A. Vananroye, W. Thielemans, C. Bartic and M. P. Lettinga. Stress-controlled shear flow alignment of collagen type I hydrogel systems. Acta Biomater. **2022**;150:128.

[61] M. Cadenas de Llano-Pérula, C. Zong, J. Van Dessel, A. M. Kuijpers-Jagtman and G. Willems. 3D quantification of in vivo orthodontic tooth movement in rats by means of micro-computed tomography. Clinical Oral Investigations. **2022**.

[62] J. Van Dessel, L. F. P. Nicolielo, Y. Huang, W. Coudyzer, B. Salmon, I. Lambrichts and R. Jacobs. Accuracy and reliability of different cone beam computed tomography (CBCT) devices for structural analysis of alveolar bone in comparison with multislice CT and micro-CT. European journal of oral implantology. **2017**;10(1).

[63] M. Chatterjee, F. Faot, C. Correa, J. Duyck, I. Naert and K. Vandamme. A robust methodology for the quantitative assessment of the rat jawbone microstructure. Int J Oral Sci. **2017**;9(2):87.

Table of Contents

AuNPs are synthesized as AuNP–Poly-L-lysine hydrobromide–rhodamine B isothiocyanate nanocomplexes and used as a pretreatment for hPDLSCs *in vitro*. The biomimetic periodontal ligament transplantation is fabricated by the pretreated hPDLSCs embedded in type-I collagen hydrogel scaffold and applied in an animal model of alveolar bone loss. The transplantation significantly promoted bone regeneration and protected bone morphometry.

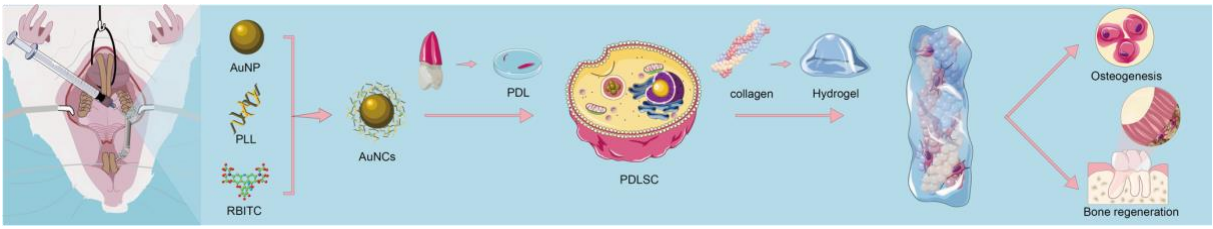

Supporting Information

Supplementary Figure 1.

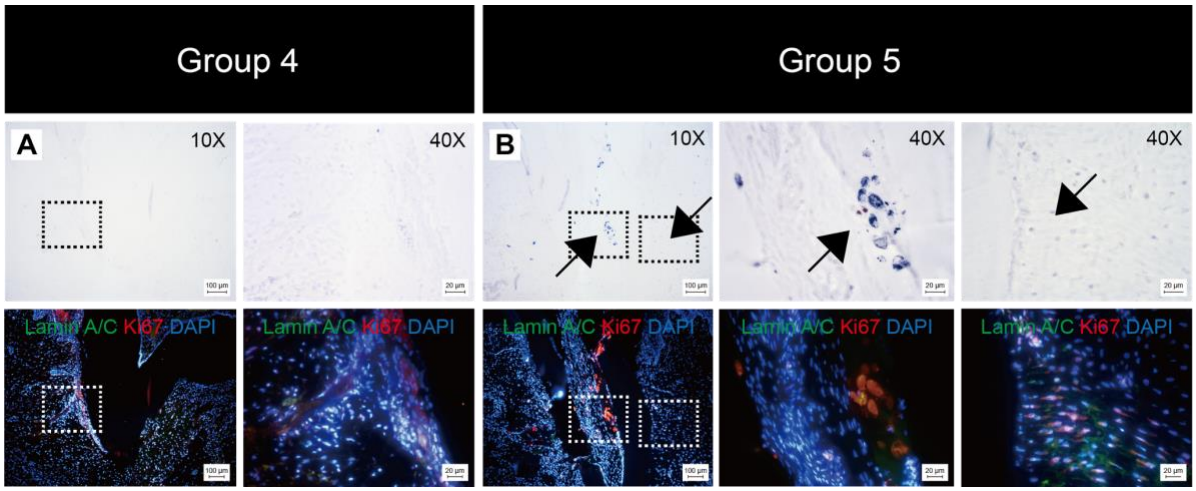

A, B) Brightfield (upper row) and fluorescence microscopy (lower row) of the sample from Group 4 (A) and 5 (B). Blue = DAPI, Green = Lamin A/C, Red = Ki67. Black arrows indicate the transplanted hPDLSCs with intracellular AuNCs. White boxes on the 10x-magnification images indicate the location of the 40×-magnification images.

Supplementary Table 1. Antibodies

Antibody	Isotype	Host	Target	Label	Company	Category number	Dilution
CD29	IgG1, k	mouse	human	FITC	eBioscience	11-0299-42	1/100
CD31	IgG1	mouse	human	PE	Immunotools	21270314	1/100
CD34	IgG1	mouse	human	PE	Immunotools	21270344	1/100
CD44	IgG2b	mouse	human	PE	Immunotools	21270444	1/100
CD45	IgG1, k	mouse	human	PE	eBioscience	12-0459-41	1/100
CD73	IgG1, k	mouse	human	FITC	eBioscience	11-0739-41	1/100
CD90	IgG1, k	mouse	human	FITC	eBioscience	11-0909-42	1/100
CD105	IgG1, k	mouse	human	PE	eBioscience	12-1057-41	1/50
OPG	IgG	rabbit	human, rat	N/A	Thermo Fisher Scientific	PA5-86053	1/100
RANKL	IgG1	mouse	human, rat	N/A	Thermo Fisher Scientific	MA1-41161	1/100
LC3A/3B	IgG	rabbit	human, rat	N/A	Thermo Fisher Scientific	PA1-16931	1/300
Beclin 1	IgG	sheep	human, rat	N/A	Thermo Fisher Scientific	OSA00006W	1/1000
P62	IgG2a	mouse	human, rat	N/A	Thermo Fisher Scientific	MA5-31498	1/500
Ki67	IgG	rabbit	human	N/A	Thermo Fisher Scientific	PA5-114437	1/100
Lamin A/C	IgG1	mouse	human	N/A	Sigma-Aldrich	SAB4200422	1/1000
Goat IgG	IgG (H+L)	goat	mouse	AF488	Thermo Fisher Scientific	A-21202	1/100
Donkey IgG	IgG (H+L)	donkey	sheep	Cy3	Jackson ImmunoResearch	713-165-003	1/400
Goat IgG	IgG (H+L)	goat	rabbit	AF633	Thermo Fisher Scientific	A-21070	1/400

Supplementary Table 2. Primer sequences used for RT-qPCR gene expression analysis

Gene	Forward primer	Reverse primer
ALP	AACCCCAGACCCTGAGTACC	CATGAGATGGGTCACAGACG
COL1	ATGACTATGAGTATGGGGAAGCA	TGGGTCCCTCTGTTACACTTT
OSTERIX	CCTCTGCGGGACTCAACAAC	AGCCCATTAGTGCTTGTAAAGG
RUN2	GGTTAATCTCCGCAGGTCACT	CACTGTGCTGAAGAGGCTGTT
LC3	CCTGTCCTGGATAAGACCAAGTT	CTCCTGTTCATAGATGTCAGCGAT
P62	CTCTCATAGCCGCTGGCTTC	CCTCAATGCCTAGAGGGCTG
GAPDH	ATGGGGAAGGTGAAGGTCG	GGGGTCATTGATGGCAACAATA